IMMOBILIZATION OF MERCURY USING

IRON SULFIDE MINERALS

Except where reference is made to the work of others, the work described in this thesis is my own or was done in collaboration with my advisory committee. This thesis does not include proprietary or classified information.

_____

Julia Michelle Bower

Certificate of Approval:

_____	_____
Willie F. Harper Assistant Professor Civil Engineering	Mark O. Barnett, Chair Associate Professor Civil Engineering
_____	_____
Dongye Zhao Associate Professor Civil Engineering	Joe F. Pittman Interim Dean Graduate School

IMMOBILIZATION OF MERCURY USING IRON SULFIDE MINERALS

Julia Michelle Bower

A Thesis

Submitted to

the Graduate Faculty of

Auburn University

in Partial Fulfillment of the

Requirements for the

Degree of

Master of Science

Auburn, Alabama
August 4, 2007

IMMOBILIZATION OF MERCURY USING

IRON SULFIDE MINERALS

Julia Michelle Bower

_____
Signature of Author

_____
Date of Graduation

THESIS ABSTRACT

IMMOBILIZATION OF MERCURY USING

IRON SULFIDE MINERALS

Julia Michelle Bower

M.S., August 4, 2007
(B.S. Auburn University, 2005)

95 Typed Pages

Directed by Mark O. Barnett

Mercury is a pervasive pollutant that has caused environmental and health problems throughout the world. Numerous industries including coal-fired power plants and chlor-alkali plants have discharged mercury into the environment. A common remediation technique at contaminated sites has been excavation and incineration of soils, which is costly and can emit harmful mercury vapor. An alternative approach is in situ immobilization of subsurface mercury using iron sulfide minerals.

In this study, pyrite was chosen for mercury immobilization studies because it is the most abundant metal sulfide in nature. Iron monosulfide (FeS) was selected because the Fe^{2+} has been shown to readily exchange with Hg^{2+} to form HgS(s). Additionally, both of these minerals are known as scavengers of mercury in the environment.

Batch experiments were conducted to investigate the kinetic and thermodynamic parameters involved in Hg(II) immobilization. Parameters such as pH, reaction time, and initial Hg(II) concentration were varied to determine optimal conditions. Batch studies revealed that both of these minerals can effectively remove Hg(II) from aqueous solution along a broad pH range. Additionally, the Hg(II) removal rates for both pyrite and FeS(s) increased with increasing pH. FeS(s) was found to be more efficient at removing Hg(II), most likely due to the formation of HgS(s).

Column experiments were conducted to provide insight into the environmental behavior of Hg(II) under dynamic (flow) scenarios. Furthermore, models were generated using CXTFIT (version 1.0.001) to aid in the development of long-term barrier systems, such as permeable reactive barriers (PRBs). Column studies revealed that transport of the Hg(II) was significantly retarded in the presence of pyrite, indicating its ability as a potential barrier material. Due to nonequilibrium, the local linear equilibrium (LLE) model over predicted the BTCs; however, the presence of an irreversible fraction of Hg(II) on the pyrite acted to counteract the increased mobility. The asymmetric shape of the BTCs, which is indicative of rate-limited and/or non-linear adsorption, corresponded with the findings of the kinetic and equilibrium batch experiments.

ACKNOWLEDGEMENTS

The author would like to acknowledge the excellent instruction, support, and guidance of her advisor, Dr. Mark Barnett. Additional thanks to Dr. Dongye Zhao and Dr. Willie Harper for their knowledge and support during the author's term at Auburn University. The author would like to thank Jinling Zhuang for his technical assistance and training in the environmental laboratory at Auburn University. The author would like to acknowledge the EPA (Grant Number GR832212) for providing financial support for the author's term at Auburn University.

Style manual or journal followed: Auburn University Graduate School: Guide to Preparation and Submission of Theses and Dissertations.

Computer software used: Microsoft Office XP: Excel, PowerPoint, Word; VisualMINTEQ; and CXTFIT

TABLE OF CONTENTS

LIST OF TABLES

LIST OF FIGURES

CHAPTER ONE

INTRODUCTION

1.1 Problem Statement

Mercury pollution is a growing concern due to its neurological health effects and vast prevalence in the environment. It is listed as one of EPA's priority persistent bio-accumulative toxins (PBTs) and is among the top five metals that most frequently exceeds ecological screening criteria at DoD sites (Salatas et al. 2004). Mercury management and remediation is necessary for the protection of the environment and promotion of better health.

1.2 Objectives

The primary objectives of this research were to gain an improved understanding of the capabilities for subsurface mercury immobilization using iron sulfide minerals. Little research has been conducted to successfully design models and field-scale systems, such as permeable reactive barriers, for in situ mercury immobilization. Therefore, batch and column experiments were carried out to effectively develop these methods. Results from the batch experiments were utilized to determine the kinetic and thermodynamic chemistry involved in immobilization. Parameters such as sulfide quantity, mercury concentration, pH, and reaction kinetics were considered. The information obtained from

the batch tests was then put to use in flow-through column studies. Column experiments simulate contaminated groundwater flow and provide insight to the immobilization behavior under hydrodynamic conditions. Furthermore, models were generated using CXTFIT (version 1.0.001) to predict the capability of barrier systems over extended periods. Solid phase characterization using XRD permitted analyses of mechanisms involved in Hg(II) removal by the iron sulfide minerals.

1.3 Organization

The organization of this report follows the guidelines for a publication-style thesis as outlined in the *Guide to Preparation and Submission of Theses and Dissertations* by the Auburn University Graduate School. Chapter 2 contains a literature review. The results of the mercury immobilization studies are divided into chapters 3 and 4. Chapter 3 contains the results from the mercury immobilization using pyrite, while Chapter 4 assesses the mercury immobilization effectiveness of FeS(s). Chapters 3 and 4 are prepared as draft manuscripts for journal submission.

CHAPTER TWO

LITERATURE REVIEW

2.1 Risk

Mercury pollution is a growing concern due to its neurological health effects and vast prevalence in the environment. Mercury has sparked much interest in the past decades, resulting in an increase of research and articles. It is listed as one of EPA's priority persistent bio-accumulative toxins (PBTs) and is among the top five metals that most frequently exceeds ecological screening criteria list at DoD sites (Salatas et al. 2004). In order to protect our natural environment and human health, mercury contamination must be controlled and reduced.

2.2 General Chemistry of Mercury

Mercury can undergo complex physical and chemical transformations, which determine its reactivity, mobility, and bioaccumulation. Elemental mercury (Hg^0) is the only metal that is liquid at room temperature. It is a less toxic species than other forms of mercury such as soluble inorganic mercury species (Hg(II)) and organic methyl mercury (MeHg) because it has little tendency to dissolve in water and is relatively unreactive. However, it can volatilize easily into a gas (Morel et al. 1998; Han et al. 2003). Most of the gaseous mercury in the atmosphere is in the form of Hg^0, but it can

be oxidized to Hg(II) by the ozone. The Hg(II) returns to land and water by precipitation. Hg(II) is reduced back to Hg^0 by both microorganisms and photoreduction (Morel et al. 1998; Amyot et al. 2005).

Soluble inorganic mercury species usually occur as Hg(II) complexed with hydroxides and chlorides, depending on pH and chloride concentration (Morel et al. 1998). In sulfidic waters, Hg(II) is found complexed with sulfide and bisulfide as well (Morel et al. 1998). These species are easily mobilized and are the most common forms of mercury that become methylated. Both MeHg and soluble inorganic mercury contribute to the major portion of mercury contamination in water, soil, and living organisms (Morel et al. 1998; Jay et al. 2000).

Methyl mercury (MeHg) is a highly toxic mercury species that can bioaccumulate, making it a primary environmental concern. The accumulation of MeHg in aquatic systems poses the greatest threat to marine life and, as a result, humans (Morel et al. 1998). The EPA (1997) affirmed in their report to congress that the primary path of human exposure to mercury is through the consumption of fish and shellfish contaminated with MeHg. Methylation occurs when a methyl group (CH_3) bonds to the mercury ion as shown below

$$CH_3 + Hg^+ \rightarrow CH_3Hg^+ . \tag{2.1}$$

Research has shown that sulfate reducing bacteria (SRB) are the primary biological contributors of MeHg formation (Morel et al. 1998; King et al. 2002; Benoit et al. 2003). SRB act as enzymes to kinetically catalyze the mercury to methylate (King et al. 2000). Microbial uptake of mercury is a key step in its bioaccumulation as well.

Microorganisms at the bottom of the food chain intake and retain MeHg. The MeHg is then biomagnified as larger organisms consume smaller ones. In fish, MeHg absorbs quickly to the walls of the intestines. Inorganic mercury species, on the other hand, have less of a tendency to bioaccumulate because they are adsorbed at the microvilli interface resulting in a slow uptake rate (Morel et al. 1998).

Because of mercury's high affinity for sulfide, Hg(II) speciation in reducing environments is controlled by sulfide complexes. Polysulfides such as HgS_x dominate the Hg-sulfide speciation at low pH and hydroxyl polysulfide species such as HgS_xOH^- form at high pH (Jay et al. 2000). In addition, Hg(II) readily converts to solid mercuric sulfide, HgS(s), in the presence of sulfides. HgS(s) is the least toxic mercury species (Svensson et al. 2006b). It is kinetically stable in soils and recognized as the particulate mercury sulfide species that controls Hg(II) solubility in anoxic waters (Charnock et al. 2003). Two polymorphs of HgS(s) exist including metacinnabar, the black form, and cinnabar, the red form; both of which have very low solubility product constants. Metacinnabar is stable at high temperatures and has a cubic structure, while cinnabar is stable at lower temperatures and has a triagonal structure (Morel et al. 1998; Charnock et al. 2003). Metacinnabar has been accepted as the stable phase in anoxic environments, whereas cinnabar in commonly found as an ore mineral (Barnett et al. 1997). Although HgS(s) is very stable, mercury can be remobilized from this solid form in the presence of excess sulfide because various water-soluble mercury-sulfide complexes can form. Furthermore, total soluble mercury has been found to increase with increasing pH and sulfide concentration (Jay et al. 2000).

2.3 Sources of Mercury Release

The cycling of mercury in the environment is very complex. Figure 1 illustrates the biogeochemical mercury cycle in air water and soil (Pierce 2007). Several steps are involved in this cycle including mercury degassing, conversion, deposition, precipitation, adsorption, and bioaccumulation. Hg^0 is released as a gas as a result of environmental and human activities, and this gas is transported through the atmosphere. In the atmosphere, Hg^0 is converted to soluble inorganic Hg(II). This mercury is then deposited on the land and surface waters. The deposited mercury can be adsorbed onto sediment particles or react with sulfides to convert to insoluble mercuric sulfide. The mercury can also bioaccumulate in terrestrial and aquatic food chains, as well as be reemitted into the atmosphere.

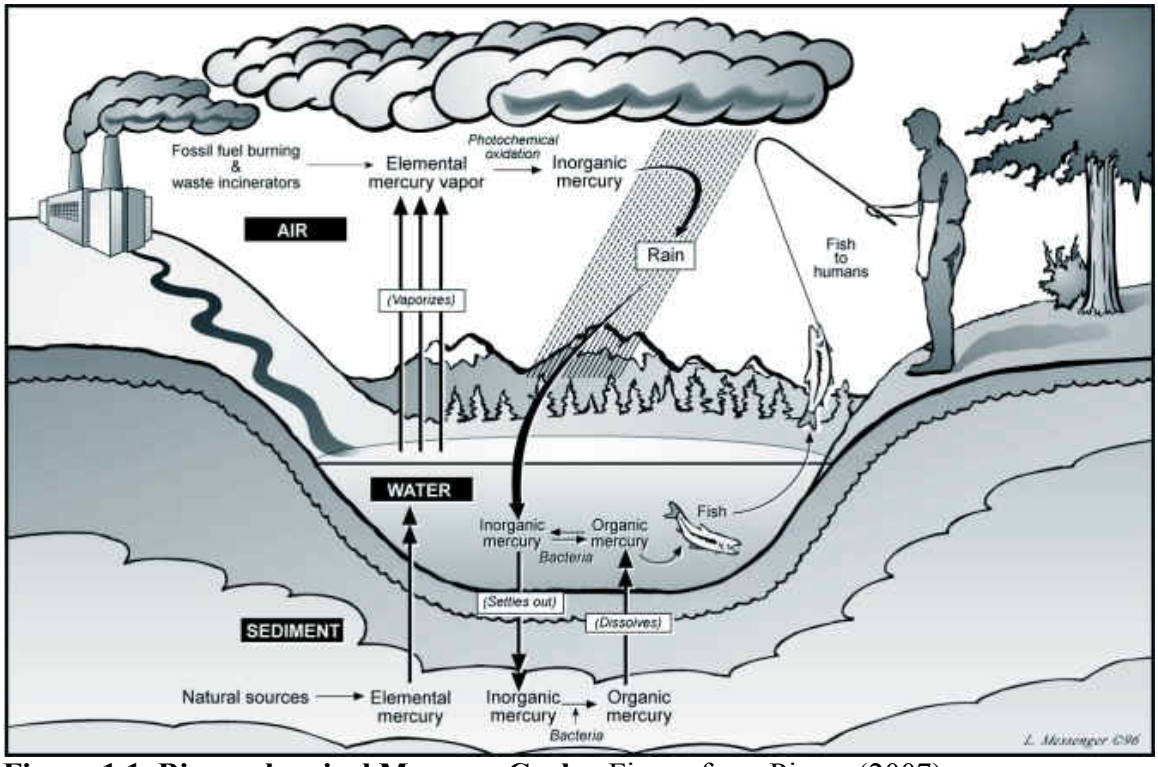

Figure 1.1. Biogeochemical Mercury Cycle. Figure from Pierce (2007).

The three major sources of mercury emissions include natural, anthropogenic, and re-emitted mercury (USEPA 1997). Natural sources of mercury are mainly found in mineral deposits and volcanoes. Anthropogenic contamination results primarily from coal-fired power plants and chlor-alkali plants (USEPA 1997; Matlock et al. 2003; Yudovich and Ketris 2005). Coal naturally contains mercury; therefore, mercury vapor is released into the atmosphere when it is burned. Mercury cells have been commonly used in the chlor-alkali process, resulting in mercury volatilization and liquid waste. Mercury cells are used in many batteries as well. Mercury is also used in laboratory and electrical equipment because of its high specific gravity and electrical conductivity. This equipment is normally disposed of by incineration or combustion, resulting in mercury air emissions. Natural or anthropogenic mercury can be re-emitted into the atmosphere by biologic and geologic remobilization processes. It has been estimated that the total mercury emissions from anthropogenic sources is about 158 tons annually (USEPA 1997).

2.4 Mercury Remediation Methods

Precipitation, adsorption, and ion exchange processes have been widely used to remediate mercury in contaminated waters. Precipitation of mercury to HgS(s) using hydrogen sulfide or alkali metals sulfide salts is a common method used for treatment of mercury in wastewater. It has been reported that sulfide precipitation can achieve up to 99.9% mercury removal (Ebadian 2001). Adsorption using activated carbon is another popular method of remediation for industrial waste. Carbon pretreated with carbon disulfide solution and sulfur-impregnated carbon were found to achieve the highest

removal levels because of the strong affinity of mercury to sulfur. More recently, ion exchange resins have been used to treat mercury-contaminated industrial wastewater. Generally, cation exchange resins containing ions such as calcium or magnesium are readily exchanged for cationic mercury. When the waste is high in chloride content, such as chlor-alkali waste, anion exchange resins are used because mercury complexes strongly with chloride, resulting in negatively charged mercury species (USEPA 1997; Ebadian 2001).

In an effort to remediate mercury at contaminated sites, soils sites have commonly been excavated and incinerated. However, this is often not economically feasible and may result in mercury air emissions (Piao and Bishop 2006). A more recent approach has been chemical leaching using oxidizing agents such as acids. The problem with this method is the expense of processing the leachant to recover the leached mercury and recycling or disposing of the mercury and treated soil (Ebadian 2001). Furthermore, both of these processes require unearthing of the contaminated soils, which is costly. Moreover, Hg^0 in soils exists as a dense non-aqueous phase liquid (DNAPL) with a high surface tension, and disturbing the soils often causes the contamination to spread. An alternative solution is in situ immobilization of mercury using sulfide minerals.

Sulfide minerals have great thermodynamic potential for mercury immobilization because mercury has a high affinity for sulfide. The most common sulfide minerals are in the form of iron sulfide, such as pyrite (FeS_2), pyrrhotite ($Fe_{1-x}S_x$), Troilite (FeS) and mackinawite (FeS) (Rickard 1969). Studies have been conducted at mercury contaminated sites in which these mercury-rich iron sulfides have been found in sediments, revealing that mercury is naturally removed by these minerals (Huerta-Diaz

and Morse 1992; Wolfenden et al. 2005). Research has also shown that iron sulfides can effectively remove mercury from aqueous solution along a wide pH range (Brown et al. 1979; Jean and Bancroft 1986; Morse and Arakaki 1993; Ehrhardt et al. 2000; Behra et al. 2001). Furthermore, immobilization of mercury by sulfide minerals is currently among the most commonly used techniques for removing inorganic mercury from wastewater (Piao and Bishop 2006).

2.5 Mercury Immobilization Mechanisms

Immobilization of mercury can occur by precipitation/coprecipitation, solid solution formation, or sorption as surface complexes on the metal sulfides (James and MacNaughton 1977). Table 1 was taken from Morse and Luther (1999) to describe the possible reactions for the incorporation of mercury into pyrite and FeS(s).

Table 2.1. Mercury Reactions with Pyrite and FeS(s).

FeS	
Hg adsorption onto FeS(s)	$FeS(s) + Hg^{2+} \rightarrow Fe - S–Hg^{2+}$
Hg inclusion into FeS(s)	$Fe – S–Hg^{2+} \rightarrow Fe(Hg)S$
HgS(s) formation	$FeS(s) + Hg^{2+} \rightarrow HgS(s) + Fe^{2+}$
FeS_2	
Hg adsorption onto pyrite	$FeS_2(s) + Hg^{2+} \rightarrow Fe - S - S–Hg$
Hg inclusion into pyrite	Fe - S – S–Hg → Fe(Hg)S2

When precipitation occurs, the result is a substitution reaction in which mercury reacts with the metal sulfide, replacing the metal, to form HgS(s) or other Hg-S solids. Precipitation of HgS(s) is expected because HgS(s) is less soluble than iron sulfides and Hg(II) has a much larger ionic radius than Fe(II) (Jeong 2005). Mercury sorption occurs when the metal sorbs onto the surface of the sulfide mineral, removing the mercury from

aqueous solution. Sorption takes place because mercury is a soft Lewis acid and thus has a strong affinity for ligands containing sulfur (Morel 1993). The most common explanation for mercury removal from solution by metal sulfides is by the formation of HgS(s); however, this is not always the case with aqueous mercury and iron sulfides (Jean and Bancroft 1986; Behra et al. 2001).

Soluble inorganic mercury species thermodynamically favor reactions that form HgS(s) when reacting with pyrite in both acidic and alkaline conditions (Hyland et al. 1990). However, X-ray photoelectron spectroscopy (XPS) and X-ray absorption fine structure (XAFS) studies have shown that other weakly and strongly bound species are formed including Hg-chloro and Hg-sulfhydryl complexes, but not HgS(s) (Hyland et al. 1990; Ehrhardt et al. 2000; Behra et al. 2001). Behra (2001) combined $Hg(NO_3)_2$ with pyrite plates and powders. It was found that at acidic pH, ternary surface complexes $\equiv S-Hg-OH$ and $\equiv S-Hg-Cl$ were formed. Fe (hydr)oxide solid solution formed along with surface complexes between mercury and oxide as well as pyritic sulfur at basic pH. A solid formation is preferred over adsorption for immobilization purposes because the mercury is weakly bound to the pyrite when adsorbed. At low pH, some of the mercury was desorbed by weak ligands, such as Cl^-. At high pH, only strong ligands of Hg(II), such as CN^-, desorbed the mercury (Behra et al. 2001). Hyland (1990) hypothesized that HgS(s) was not formed due to the higher kinetic stability of pyrite. In addition, because mercury forms very strong chloride complexes and has a high hydrolysis constant, chloride (Cl^-) and hydroxide (OH^-) must be displaced from mercury for a sulfide mineral to form. Therefore, the mercury-sulfide reaction is retarded and the mercury incorporates into the pyrite, instead of forming HgS(s) (Morse and Luther 1999).

HgS(s) formation has been found to occur in the presence of aqueous mercury and FeS(s) (Jeong 2005; Svensson et al. 2006b). Jeong (2005) explained that environmental conditions have great implications on the chemical reactions between Hg(II) and FeS(s). It was found that adsorption of Hg(II) occurred at very low molar ratios of Hg/FeS (< 1) due to the greater availability of sorption sites. Coprecipitation of Hg-rich sulfide occurred at higher molar ratios. Fe(II) was exchanged during coprecipitation, but was readsorbed on the FeS at acidic pH and formed a precipitate at high pH, which could itself serve as an adsorbent for Hg(II). At Hg/FeS molar ratios greater than 1, formation of mercury chloride salts, Hg_2Cl_2 at acidic pH and $HgCl_2$•3HgO at basic pH, occurred due to the lack of sulfide needed for coprecipitation. In addition, both adsorbed and precipitated Hg were not easily extracted by strong ligands (Jeong 2005).

Traces of HgS(s) have been detected in samples containing Hg^0 and pyrite (Navarro et al. 2006; Svensson et al. 2006a). Anaerobic, alkaline conditions are thermodynamically less suitable for HgS(s) formation from pyrite and Hg^0, indicated by the positive Gibbs free energy (ΔG):

$$FeS_2(s) + 2Hg^0 + 2H^+ \rightarrow HgS(s) + Fe^{2+} + H_2S(aq) \qquad (2.2)$$

$$\Delta G = 10.0 \text{ kJ/mol}$$

However, oxidizing conditions result in spontaneous formation of HgS(s) from Hg^0 and pyrite, indicated by the negative ΔG.

$$FeS_2(s) + 2Hg^0 + 2H^+ + \frac{1}{2}O_2 \rightarrow 2HgS(s) + Fe^{2+} + H_2O \qquad (2.3)$$

$$\Delta G = -245.0 \text{ kJ/mol}$$

Studies have shown that the reaction of Hg^0 with FeS(s) will form HgS(s) under both anaerobic and aerobic conditions (Wolfenden et al. 2005; Svensson et al. 2006b).

$$2FeS(s) + Hg^0 + 4H^+ \rightarrow HgS(s) + 2Fe^{2+} + H_2S(aq) + H_2(g) \quad (2.4)$$

ΔG = -40.0 kJ/mol

$$FeS(s) + Hg^0 + 2H^+ + \frac{1}{2}O_2 \rightarrow HgS(s) + Fe^{2+} + H_2O \quad (2.5)$$

ΔG = -266.0 kJ/mol

2.6 Mercury-Sulfide in the Environment

The weathering of HgS(s) by simple (non-oxidative) dissolution is thermodynamically restricted due to its strong insolubility, indicated by the low equilibrium constant (K):

$$HgS(s) + 2H_2O \rightarrow Hg(OH)_2^0 + H_2S \quad (2.6)$$

$K = 10^{-38}$

However, HgS(s) is thermodynamically unstable in the presence of dissolved oxygen and other oxidants found in nature because of the existence of reduced sulfur, which results in dissolution:

$$HgS(s) + 2O_2(aq) + 2H_2O \rightarrow Hg(OH)_2^0 + SO_4^{2-} + 2H^+ \quad (2.7)$$

$K = 10^{93}$

To the degree HgS(s) can kinetically withstand oxidation, it may remain stable in the environment after it is formed, even under oxidizing conditions. (Barnett et al. 2001).

The formation of HgS(s) and other Hg-S precipitates from mercury and sulfide interactions in water, soil, and sediments provides evidence that mercury pollution can be abated. HgS(s) is less volatile than other forms of mercury, and thus potentially less harmful. It has also been proposed that HgS(s) is the primary sink for mercury in the environment (Barnett et al. 2001). However, soluble inorganic mercury and pyrite interactions do not form HgS(s); therefore, further research is necessary to determine the mechanisms and end products of mercury immobilization using pyrite. Furthermore, the effects of mercury transformation by reaction with iron sulfides on methylation have not been well documented. Mercury's environmental impact is shaped by the degree to which sulfide phases can compete with biological methylation processes and act as a sink for mercury.

2.7 Pyrite Oxidation

The chemical nature and speciation of mercury is heavily influenced by redox conditions as previously discussed. This is also the case with mercury bound to pyrite. Huertaz Diaz and Morse (1992) found that sedimentary pyrite can be a significant sink for mercury. The oxidation of pyrite, however, can cause pyritized metals to become displaced from the pyrite. Sedimentary pyrite can be oxidized during resuspension, dredging, and bacterial migration (Morse 1994).

Pyrite and other iron sulfides have been heavily associated with acid mine drainage (AMD). AMD is a strongly acidic solution containing high amounts of heavy metals and sulfate, which threatens surface water and groundwater quality. When pyrite is exposed to the environment during mining and excavation, it reacts with oxygen and

water to form sulfuric acid, resulting in acid mine drainage. Pyrite oxidation can be mediated chemically or biologically. Pyrite oxidation by oxygen is kinetically slow and is shown below.

$$FeS_2 + 3.5O_2 + 3H_2O \rightarrow Fe^{2+} + 2SO_4^{2-} + 2H^+ \quad (2.8)$$

Pyrite oxidation is microbially catalyzed by *Thiobacillus ferrooxidans*. These bacteria generate their energy by oxidizing Fe^{2+} to Fe^{3+}. Pyrite is then oxidized by ferric iron (Fe^{3+}), which is kinetically faster than pyrite oxidation by oxygen. The pyrite oxidizes to produce ferrous iron (Fe^{2+}) and sulfate (SO_4^{2-}) as shown below.

$$FeS_2 + 14Fe^{3+} + 8H_2O \rightarrow 15Fe^{2+} + 2SO_4^{2-} + 16H^+ \quad (2.9)$$

(Blodau 2006).

The effects of mercury and iron sulfide reactions should be studied further with respect to mercury methylation as well. Studies have shown that sulfate-reducing bacteria are the main promoters of mercury methylation. Research has also suggested that methyl mercury (MeHg) levels increase with increasing sulfate concentration (Morel et al. 1998; Benoit et al. 2003). Behra (2001) reported measuring sulfates in solution at both acidic and alkaline conditions due to the oxidative dissolution of pyrite. Furthermore, experiments conducted with and without Hg(II) resulted in the same released species from oxidative dissolution of pyrite. However, it was also found that pyrite oxidation was limited in the presence of Hg(II) (Bonnissel-Gissinger et al. 1998).

2.8 Comparison of Iron Sulfide Minerals

The literature reveals FeS(s) to be a more suitable immobilizer than pyrite for Hg(II). Research has shown that Hg is much more easily extracted from pyrite than from

FeS(s) in both adsorbed and precipitated forms. In addition, solid phase characterization reveals HgS(s) and other precipitates are formed on FeS(s) in most conditions, while precipitates are formed on pyrite only in very basic conditions. Furthermore, Behra (2001) found that pyrite has a sorption capacity of 2 mg Hg(II) g^{-1}, while Jeong (2005) found that FeS(s) has a sorption capacity of 46 mg Hg(II) g^{-1} and Brown (1979) found a maximum adsorption capacity of 59 mg Hg(II) g^{-1} for FeS(s).

CHAPTER THREE

IMMOBILIZATION OF MERCURY BY PYRITE

3.1 Introduction

Mercury pollution is a growing concern due to its neurological health effects and vast prevalence in the environment. It is listed as one of EPA's priority persistent bio-accumulative toxins (PBTs) and is among the top five metals that most frequently exceeds ecological screening criteria at DOD sites (Salatas et al. 2004). In order to protect our natural environment and human health, mercury contamination must be controlled and minimized.

Mercury contamination originates from both natural and man-made sources. Natural sources of mercury are mainly found in mineral deposits, while man-made contamination results primarily from coal-fired power plants and chlor-alkali plants (Matlock et al. 2003; Yudovich and Ketris 2005). In an effort to remediate the problem at contaminated sites, mercury laden soils have been excavated and incinerated. However, this is often not economically feasible and can result in mercury air emissions. Furthermore, disturbing the soils often causes the contamination to spread (Piao and Bishop 2006). An alternative approach is in situ immobilization of mercury using sulfide minerals.

Sulfide minerals have great thermodynamic potential for mercury immobilization because mercury has a high affinity for sulfide (Brown et al. 1979; Gustin et al. 2002). The most common sulfide minerals are iron sulfides, such as pyrite (FeS_2), pyrrhotite ($Fe_{1-x}S_x$), and mackinawite (FeS). Pyrite was the sulfide mineral chosen as a target immobilizer of mercury because it is the most abundant metal sulfide in nature (Behra et al. 2001). In addition, studies have been conducted on anoxic marine sediments in which mercury-rich pyrite has been found, revealing that mercury is naturally removed by this mineral (Huerta-Diaz and Morse 1992). Research has also shown that pyrite can effectively remove mercury from aqueous solution along a wide pH range (Brown et al. 1979; Morse and Arakaki 1993; Ehrhardt et al. 2000; Behra et al. 2001).

Immobilization of mercury by sulfides can occur by precipitation/coprecipitation, sorption as surface complexes on the metal sulfides, and solid solution formation (Morel 1993). When precipitation occurs, the result is a substitution reaction in which mercury reacts with the metal sulfide, replacing the metal, to form a mercury sulfide solid (Morel 1993). Mercury sorption occurs when the mercury sorbs onto the surface of the sulfide mineral, removing the mercury from aqueous solution, rather than forming mercuric sulfide (HgS(s)). Sorption takes place because mercury is a soft Lewis acid and thus has a strong affinity for ligands containing sulfur (Ehrhardt et al. 2000). HgS(s) is the most common solid that forms when mercury reacts with metal sulfides. The formation of HgS(s) from mercury and sulfide interactions in water, soil, and sediments provides evidence that mercury pollution can be abated. HgS(s) is relatively insoluble and less volatile than other forms of mercury, and thus potentially less harmful (Barnett et al.

2001). It has also been proposed that HgS(s) is the primary sink for mercury in the environment (Stein et al. 1996).

X-ray photoelectron spectroscopy (XPS) studies have been conducted on mercury-pyrite interactions to determine the sorption mechanisms. Research has shown that weakly and strongly bound species are formed including Hg-chloro and Hg-sulfhydryl complexes, but not HgS(s) (Hyland et al. 1990; Ehrhardt et al. 2000; Behra et al. 2001). It has been hypothesized that this is due to the higher kinetic stability of pyrite than other sulfide minerals (Hyland et al. 1990). In addition, because mercury forms very strong chloride complexes and has a high hydrolysis constant, chloride (Cl^-) and hydroxide (OH^-) must be displaced from aqueous mercury for HgS(s) to form. Therefore, the mercury incorporates into the pyrite, rather than forming of HgS(s) (Morse and Luther 1999). More recently however, traces of HgS(s) have been detected in samples containing elemental mercury (Hg^0) and pyrite (Navarro et al. 2006; Svensson et al. 2006a).

The objectives of this study were to gain an improved knowledge of the potential for subsurface mercury immobilization using pyrite. This was achieved by analysis of the kinetic and thermodynamic chemistry involved in the immobilization of aqueous Hg(II) by pyrite using batch tests and examining this behavior under hydrodynamic conditions through column experiments. Kinetic tests results revealed the rates by which the reactions took place. Equilibrium experiments were carried out to determine isotherm curves, which were then fitted to models in order to predict sorption behavior. The information obtained from the batch tests were put to use in flow-through column studies. Column experiments simulate groundwater flow and provide insight to the

immobilization behavior under hydrodynamic conditions. Furthermore, models were generated using CXTFIT (version 1.0.001) to aid in the development and to anticipate the functionality of barrier systems over extended periods.

3.2 Materials & Methods

3.2.1 Pyrite

The pyrite used in this study was obtained from Wards Science Co. It was crushed, pulverized with a mortar and pestle, and then sieved to < 250 microns. The pyrite was washed with 0.01 M HCl to remove oxidation products and stored under anaerobic conditions until use. Removal of oxidation products and the purity of the pyrite were confirmed by X-ray diffraction (XRD). Scanning electron microscopy (SEM) was utilized to examine the morphology and size distribution of the pyrite (Fig. 3.1). The particle sizes ranged from about 1 to 250 μm, and appeared nonporous. This particle size distribution was confirmed using sieve analysis, which also revealed that the average particle size was about 75 μm. The specific surface area of the powder was determined to be 0.42 $m^2\ g^{-1}$ using Kr BET at 77 K, which is very similar to the value of 0.4 $m^2\ g^{-1}$ found by Behra (2001) for similar particles sizes.

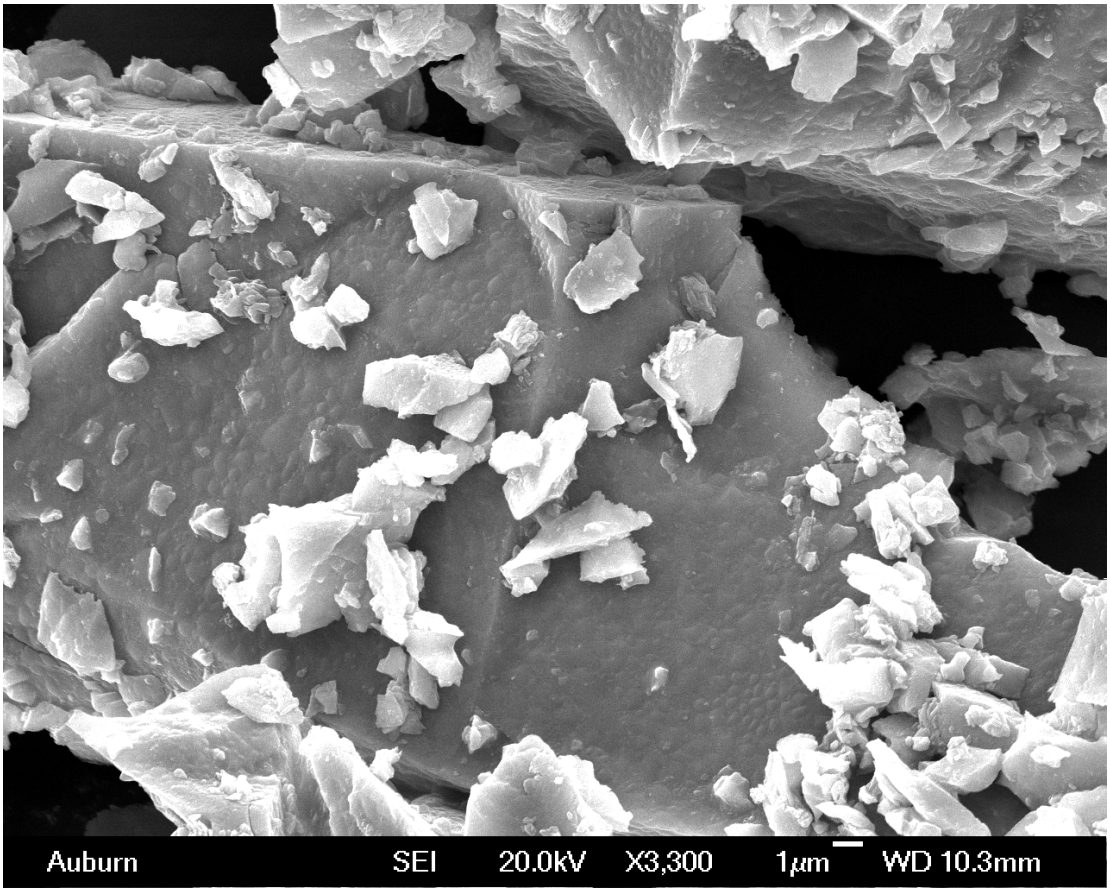

Figure 3.1. SEM photomicrograph of pyrite.

3.2.2 Batch Experiments

Batch experiments were conducted in the absence of oxygen because pyrite is thermodynamically unstable in the presence of atmospheric O_2, indicative that pyrite would not be the optimal barrier mineral in oxic groundwater. All solutions were sparged with N_2 to drive off any dissolved O_2 prior to reaction, and experiments were conducted in an anaerobic chamber.

Kinetic, isotherm, and pH edge batch experiments were performed in which the effect of reaction time, Hg(II) concentration, and pH were examined, respectively. Stock solutions of Hg(II) were prepared in a 100 mL volumetric flask using 2 mL of a standard solution of $Hg(NO_3)_2$ with a concentration of 1g L^{-1}, resulting in a 2000 μg L^{-1} Hg(II) solution. For all experiments, initial concentrations were below 10 mg L^{-1} Hg(II) to prevent HgO(s) precipitation. Adjustments in pH were made using N_2 sparged 0.05 M NaOH or HCl. Each vial contained 2 g L^{-1} pyrite. All suspensions were prepared in a constant ionic strength background matrix of NaCl (0.1 M) because Hg(II) naturally forms very strong associations with chloride ions. Additionally, the strong ligands that formed helped to stabilize the Hg(II) in solution and prevent atmospheric loses. Samples were rotated end-over-end at a rate of 8 rpm. Samples were centrifuged at 2500 g for 20 minutes at 25ºC and filtered through a 0.45 μm acrodisk syringe filter membrane to separate pyrite solids from the liquid. Sub-samples of the filtrate were taken to measure the pH of each sample.

3.2.3 Column Experiments

Column experiments were conducted to provide insight into the environmental behavior of Hg(II) under dynamic (flow) scenarios. Studies were carried out under both aerobic and anaerobic conditions, as both of these could be encountered in the field. Anaerobic conditions were achieved by bubbling the influent continuously with $N_2(g)$ to remove oxygen.

Two 1 cm diameter borosilicate glass columns were packed with 6.30 g of pure quartz sand. One column contained no pyrite (sand only), while the other column contained 0.0625 g of pyrite. This scenario was utilized to compare the breakthrough curves (BTCs) of Hg(II) with and without pyrite sorption. The barrier material consisted of 0.25 g of washed pyrite mixed with 0.75 g of the pure quartz sand; 0.25 g of this mixture was distributed evenly at the top of the column. The column was packed to a height of 5 cm, resulting in a porosity of 0.37 and a bulk density of 1.67 g cm^{-3}. A nonreactive (KBr) tracer test was also performed to determine the dispersion coefficient (D) and Peclet number (P = vL/D).

A 100 μg L^{-1} Hg(II) solution was prepared in a 1000 mL volumetric flask using 100 ml of a 1 mg L^{-1} standard solution of $Hg(NO_3)_2$ and DI water. This solution concentration was used based on the equilibrium effluent mercury concentration found in a study using 1 g Hg^0 in the sand column, not shown here. The ionic strength was fixed at 0.1 M NaCl. A four way valve was set up so that two influents could be used. The first was a 0.1 M NaCl solution at pH 4, and the second was the 100 μg L^{-1} Hg(II) 0.1 M NaCl solution at pH 4. For the tracer test, the second influent was a 0.1 M KBr solution. Using this pH, the Hg(II) solution pH remained stable without added buffering and the

results of the column experiments could be compared to batch results at corresponding pH. Additionally, this pH is similar to that found in Fe-oxide rich Ultisols common to the southeastern U.S. An infiltration rate similar to the mean stormwater flow found at Oak Ridge Reservation in Oak Ridge, TN, which accounts for over 90% of the contaminant transport in the area (Solomon 1992) was desired. Therefore, a rate of 0.076 cm min^{-1} was used. This flow rate also prevented bed disturbance and channel formation. The columns were set in run up-flow mode and samples were obtained using a fraction collector. For rate comparison purposes, a column experiment was conducted at 0.255 cm min^{-1} as well. Initially, the 0.1 M NaCl solution was used as the influent until the column was saturated; then, the valve was switched so that the 100 μg L^{-1} Hg(II) solution was the influent. Once the pyrite was saturated with Hg(II), the valve was turned back to the 0.1 M NaCl solution influent and run until the effluent concentration fell below the Hg detection limit (0.5 μg L^{-1}). The pH of each sample was recorded immediately after each collection was complete. The laboratory room temperature was recorded periodically, and remained stable at 21 ± 2ºC. Experiments were carried out in duplicate.

3.2.4 Analytical Methods

Mercury analysis was conducted by Cold Vapor Atomic Absorption Spectrophotometry (CVAAS-USEPA Methods 7470A and 7471A). Mercury sample preparation and preservation was conducted similar to these two procedures and those described in EPA Method 1631. Prior to analysis, all samples were first preserved and oxidized with 1% BrCl, followed by 1% hydroxylamine hydrochloride to destroy the unreacted BrCl. Although BrCl is mainly used for preservation of samples containing

organic matter, inconsistent results were obtained when BrCl was not utilized. Mercury has been shown to sorb to container walls and volatilize from reactors, causing significant mass balance problems. Teflon containers were used to minimize sorption to container walls. Spikes, blanks, and duplicates were run to estimate process error and quantify possible losses to containers.

Power XRD was performed on a Rigaku Miniflex Diffractometer using Cu-Kα radiation (30 kV, 15 mA). Diffraction data were collected in the range of $3^\circ < 2\theta < 90^\circ$ at a rate of 0.10° (2θ) min^{-1}. For detailed structure information, the results were analyzed using JADE (Version 6.0), a software tool for XRD powder pattern processing.

3.3 Results and Discussion

3.3.1 Batch Experiments

In order to examine the influence of pH on Hg(II) adsorption to pyrite, preliminary batch sorption studies were conducted at a constant initial Hg(II) concentration (2000 μg L^{-1}) over a pH range of 1.5 to 11.5 and a reaction time of two days (Fig 3.2). Hg(II) removal from solution increased with increasing pH, a common characteristic of cationic adsorption. Additionally, approximately constant Hg(II) removal (> 95%) was achieved above pH 5. The results correspond closely with those found by Behra (2001), who suggested that the hydrolysis of Hg(II) is required for sorption to take place. It has also been stated that Hg(II) adsorbs on sulfide minerals up to approximately one monolayer (Jean and Bancroft 1986; Behra et al. 2001). Generally, adsorption edge studies are carried out to equilibrium; however, it was found in the following kinetic experiments that equilibrium was not actually achieved at all pH values

in just two days. Due to the difference in sorption at varying pH, further batch experiments were conducted using acidic, neutral and basic pH values.

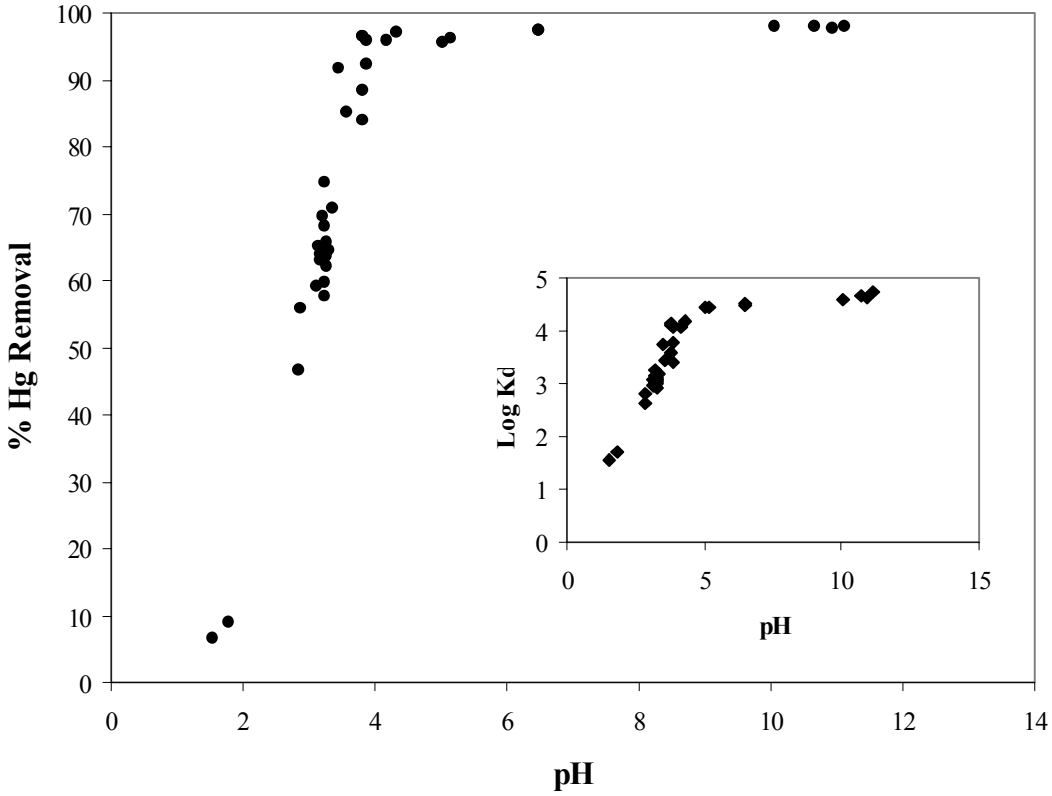

Figure 3.2. Hg(II) sorption onto pyrite as a function of pH. Initial pyrite and Hg(II) concentrations were 2 g L^{-1} and 2000 µg L^{-1}, respectively. Ionic strength was 0.1 M NaCl. pH was adjusted using 0.05 M HCl or NaOH.

Analysis of kinetics is necessary in order to determine the rate of equilibrium attainment as well as reaction mechanisms. Figure 3.3 illustrates the effect of pH and time on Hg(II) sorption onto pyrite, where the rate of sorption increases with increasing pH. In addition, sorption was initially rapid and then slows with time. This is generally attributed to high affinity sites being filled initially, then lower affinity sites being filled more slowly (Axe and Anderson 1995). These results show the reaction time to reach constant removal (> 95%) for pH 4.1 ± 0.2 is about 8 days, pH 6.4 ± 0.2 is about 2 days, and pH 10.4 ± 0.2 is about 8 hours for an initial Hg(II) concentration of 2000 μg L^{-1}. This difference in removal time with pH can be explained by the concept that the concentration of Fe hydroxide sites, which can adsorb Hg(II) at high pH, increase with pH, resulting in two types of adsorption sites (Axe and Anderson 1998; Bonnissel-Gissinger et al. 1998). Additionally, the hydroxyl-mercury complex, $Hg(OH)_2$, which is in greater concentrations at higher pH, has higher affinity for adsorption than chloride-mercury complexes, which are greater in concentration at lower pH. This is because the formation of an OH group of the mercury ion reduces the free energy required for adsorption and the presence of chloride ions retard Hg(II) sorption to pyrite (Walcarius et al. 1999; Ehrhardt et al. 2000; Behra et al. 2001).

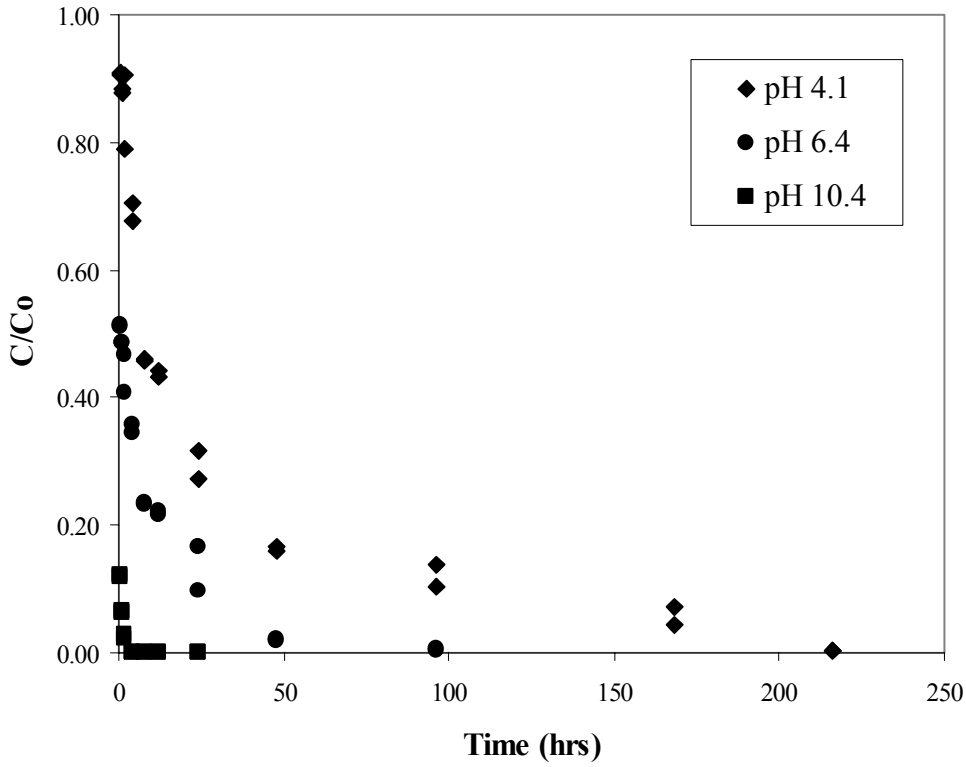

Figure 3.3. Hg(II) sorption onto pyrite as a function of time. Initial pyrite and Hg(II) concentrations were 2 g L^{-1} and 2000 μg L^{-1}, respectively. Ionic strength was 0.1 M NaCl. Experiments were carried out at pH 4.1, 6.4, and 10.4.

Transformations of Hg(II) concentration and time were performed, and it was observed that at all pH values the data could be linearized by plotting the natural log of Hg(II) concentration versus the square root of time, resulting in coefficient of determination (R^2) values greater than 0.9 for all cases (Fig 3.4). In general, when the plot of concentration versus square root of time is linear, intraparticle diffusion is present (Jenne 1998). However, no previous analysis of the plot of ln C versus square root of time was found.

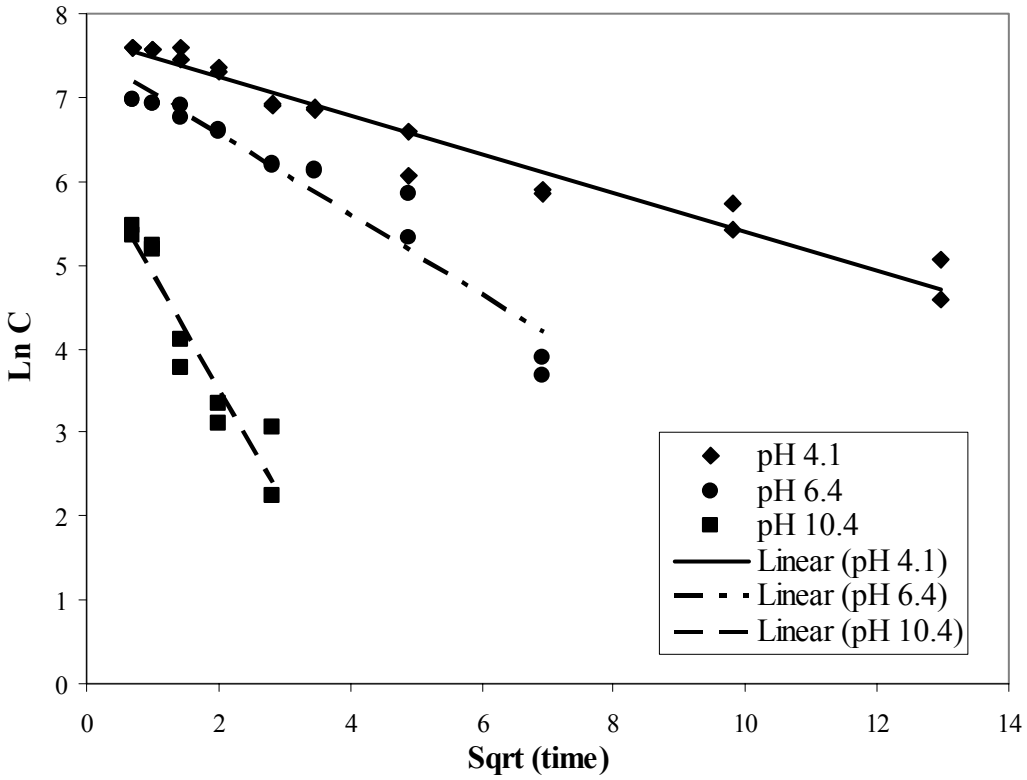

Figure 3.4. Linearization of Hg(II) sorption onto pyrite as a function of time. Initial pyrite and Hg(II) concentrations were 2 g L^{-1} and 2000 µg L^{-1}, respectively. Ionic strength was 0.1 M NaCl. Experiments were carried out at pH 4.1, 6.4, and 10.4.

Bulk diffusion, film diffusion, and intraparticle diffusion are the three stages that are involved in metal sorption onto a solid (Sparks 1989). The rate limiting steps for adsorption and ion exchange are film diffusion or intraparticle diffusion (Sparks 1989). SEM photomicrographs reveal the pyrite is nonporous (Fig. 3.1); therefore, traditional intraparticle diffusion does not seem likely. However, this does not consider Hg(II) incorporation into the pyrite lattice via diffusion. Huerta Diaz and Morse (1992) found mercury completely incorporated into the pyrite phase in anoxic marine sediments in coastal regions of the Southeastern U.S.

In order to understand sorption processes, analysis of sorption equilibrium data is required. Moreover, equilibrium isotherm models and parameters can be obtained from this data, providing insight into sorption mechanisms as well as sorbent properties. Isotherm experiments were conducted at pH values of 4.2, 6.4 and 10.4 (± 0.2) using a two day reaction time (Fig 3.5-3.9). It was determined from the batch kinetic tests that actual equilibrium times could not be determined at any pH value because the Hg(II) concentrations fell below the detection limit instead of leveling out. The same reaction time for all pH values was desired for comparison purposes; therefore, a reaction time of two days was chosen. A two day reaction time was used for the pH edge batch experiments as well. Figure 3.5 illustrates the affect of pH on sorption capacities. Much greater sorption was achieved at higher pH than lower, again, a result of mercury speciation and surface sorption sites.

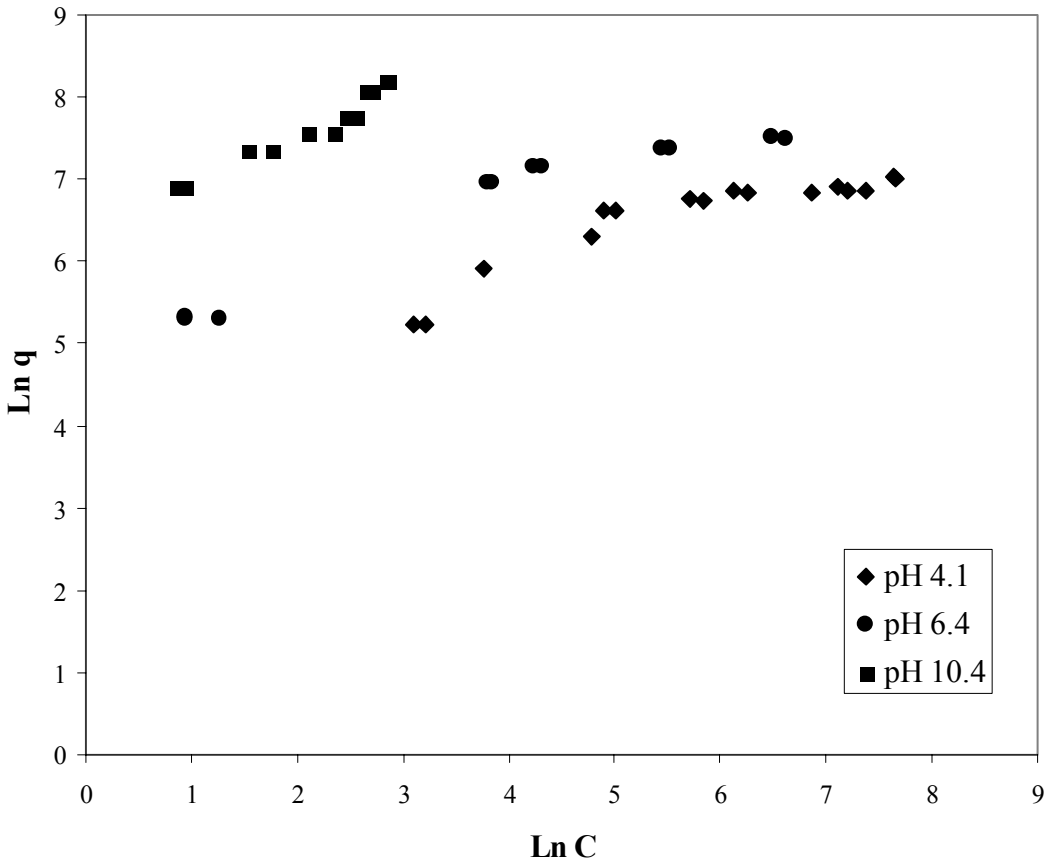

Figure 3.5. Hg(II) sorption isotherm data at pH 4.1, 6.4, and 10.4 ± 0.2. Initial pyrite concentration was 2 g L^{-1}. Initial Hg(II) concentration ranged from 400 to 8000 µg L^{-1}. Ionic strength was 0.1 M NaCl.

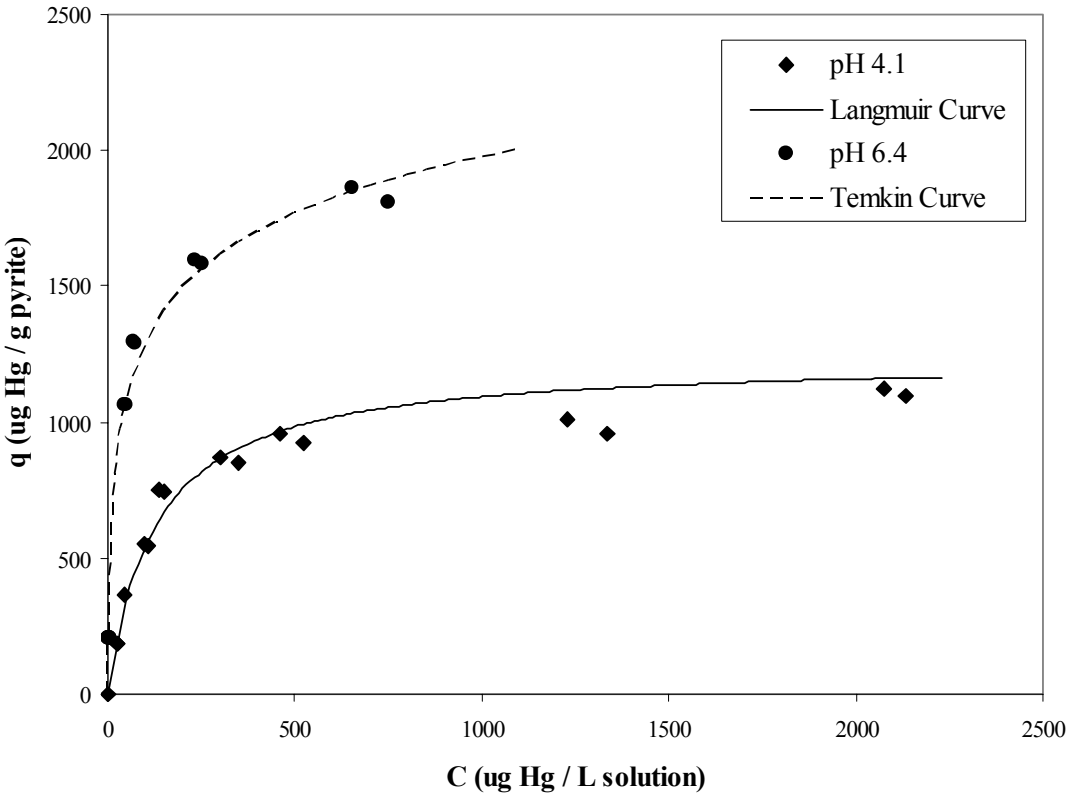

Figure 3.6. Hg(II) sorption isotherms at pH 4.1 and 6.4 ± 0.2. Initial pyrite concentration was 2 g L^{-1}. Initial Hg(II) concentration ranged from 400 to 4000 µg L^{-1}. Ionic strength was 0.1 M NaCl.

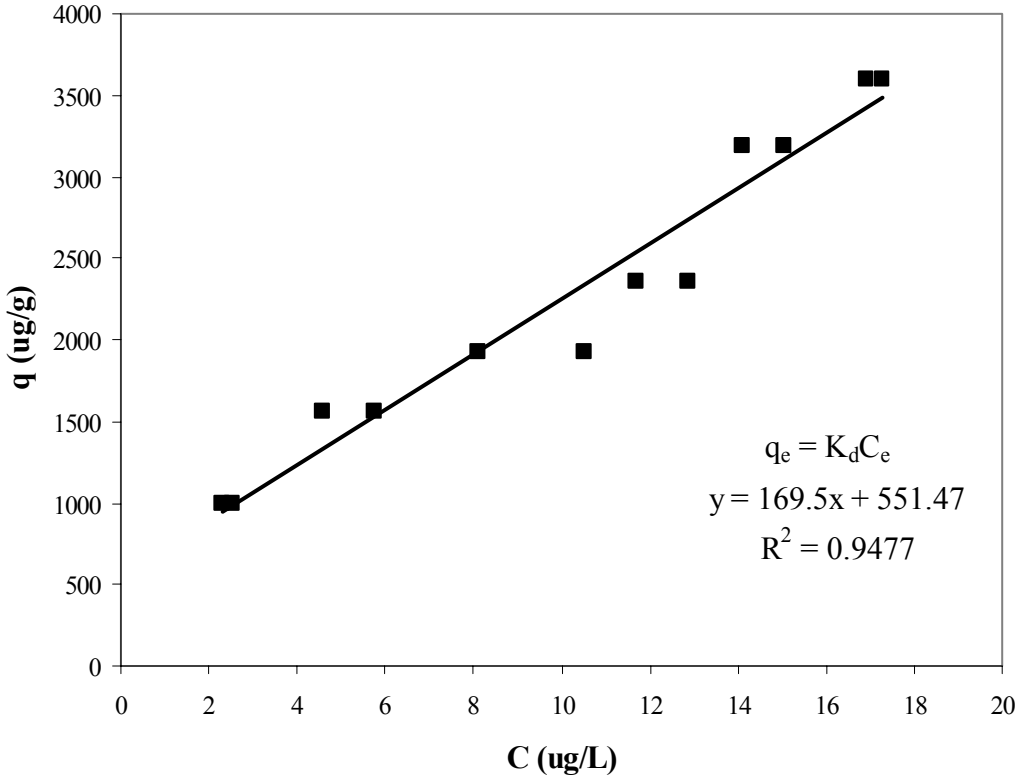

Figure 3.7. Hg(II) sorption isotherm at pH 10.4 ± 0.2. Initial pyrite concentration was 2 g L^{-1}. Initial Hg(II) concentration ranged from 2000 to 8000 µg L^{-1}. Ionic strength was 0.1 M NaCl.

Several isotherm models were employed to model the data at various pH values. The model that best fit the data was determined from the coefficient of determination (R^2) and the method of least square, or sum of square error (SSE). At pH 4.2, the Langmuir Isotherm best fit the data with an R^2 value of 0.98 and SSE = 7.66×10^{-5} (Fig 3.6, 3.8). The Langmuir Isotherm can be can be expressed by the equation:

$$q = \frac{bQC}{1 + bC} \tag{3.1}$$

where q (mg/g) is the solid phase Hg(II) concentration, b is the Langmuir affinity coefficient, Q is the maximum sorption capacity, and C is the Hg(II) concentration in the aqueous phase (Weber 2001). This equation can be solved linearly by taking the inverse of both sides and plotting (Fig 3.8). Q and b were determined to be 1230 μg Hg(II) g^{-1} pyrite and 7.92 L mg^{-1} Hg(II), respectively. Behra (2001) determined the sorption capacity to be about 2000 μg Hg(II) sorbed g^{-1} pyrite, which is slightly higher. However, this is the maximum sorption calculated at pH 4.2; greater sorption was achieved above this pH (Fig 3.2).

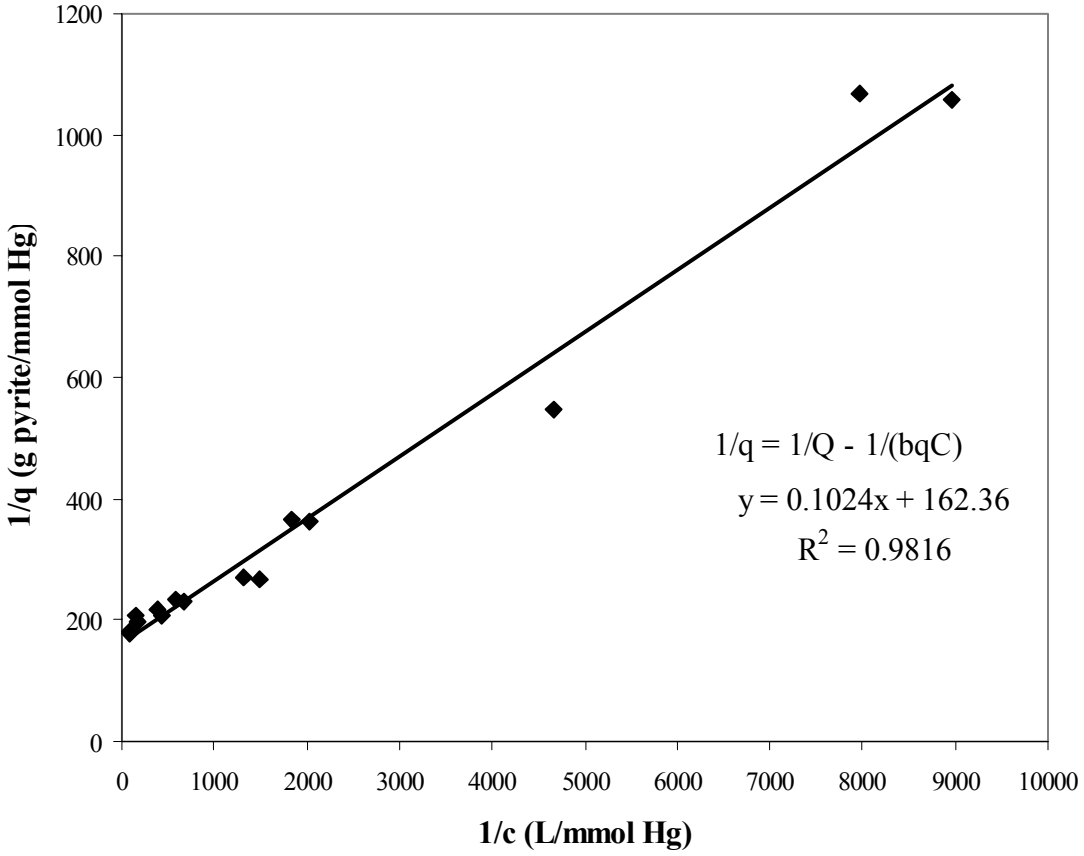

Figure 3.8. Langmuir Isotherm Model at pH 4.1 ± 0.2.

The data best fit the Temkin Isotherm at pH 6.4, with $R^2 = 0.99$ and SSE = 8.06 x 10^{-4} (Fig 3.6, 3.9). The Temkin Isotherm can be written in the form of the equation

$$q = \frac{RT}{b} \ln(AC) \tag{3.2}$$

where R is the universal gas constant (8.314 J mol^{-1} K^{-1}), T is the absolute temperature, and A and b are Temkin isotherm constants (Ho et al. 2002). This equation was solved linearly by plotting q versus ln C (Fig 3.9). An adsorption maximum is not included in the Temkin equation; however, it does appear that the data points are approaching 2000 μg Hg(II) sorbed g^{-1} pyrite, as observed by Behra (2001).

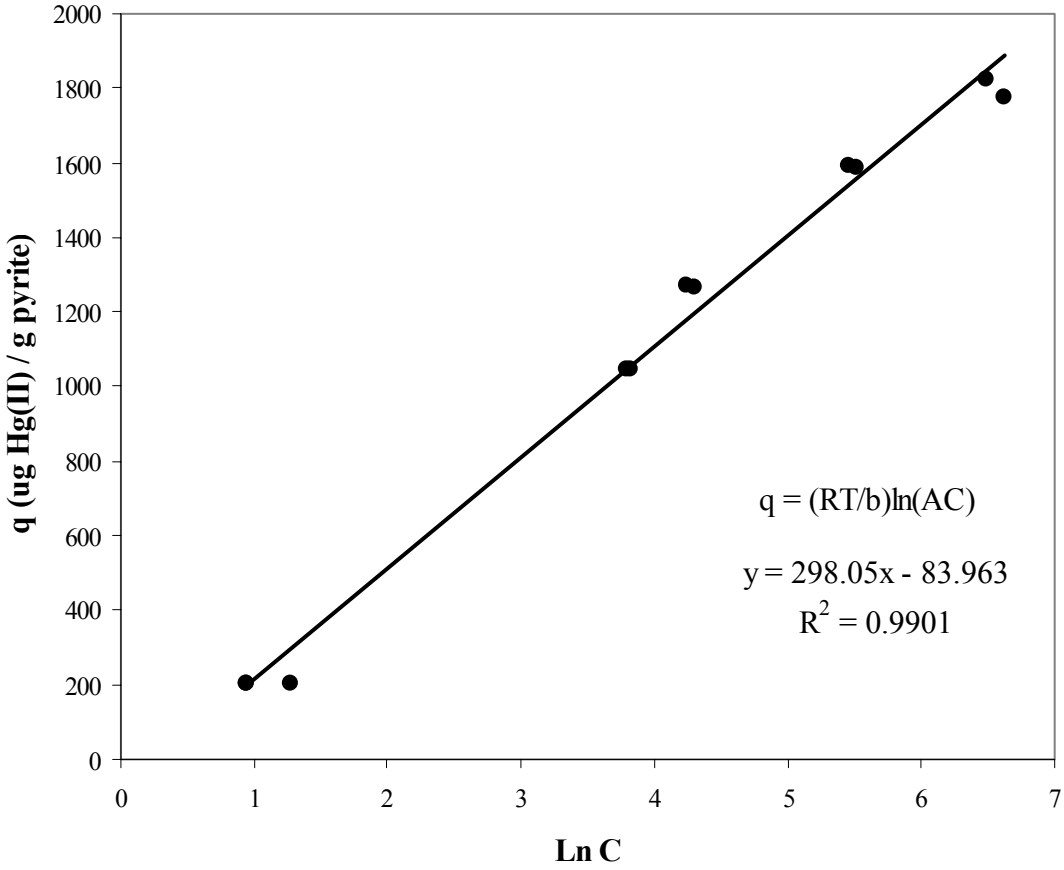

Figure 3.9. Temkin Isotherm Model at pH 6.4 ± 0.2.

At pH 10.4, the pyrite achieves great sorption (> 3500 μg Hg(II) g^{-1}). A linear isotherm best fit the data at pH 10.4, with an R^2 value of 0.95 (Fig 3.7). A linear isotherm can be modeled using the following equation

$$q_e = K_D C_e . \tag{3.3}$$

The distribution coefficient (K_D) was determined to be 169.5 L g^{-1} pyrite from the slope of the isotherm curve. Solid formation could explain the high sorption capacity. Behra (2001) found that at basic pH, both S-H and O-H groups are formed and iron hydroxides, which have the ability to sorb Hg(II), are present at the pyrite surface. Previous studies of Hg(II) adsorption to Fe hydroxides at the same ionic strength (0.1M NaCl) have found that maximum Hg(II) sorption to both HFO and goethite occurs at pH 10, with capacities of about 68,200 μg Hg(II) g^{-1} HFO (50 μmol Hg(II) m^{-2} HFO) and 220 μg Hg(II) g^{-1} goethite (7 μmol Hg(II) m^{-2} goethite) (Tiffreau et al. 1995; Bonnissel-Gissinger et al. 1999). Figure 3.10 illustrates the difference in Hg(II) sorption between pyrite and these Fe hydroxides. The ability of these iron hydroxides to adsorb Hg(II) could explain the such remarkable sorption at pH 10.

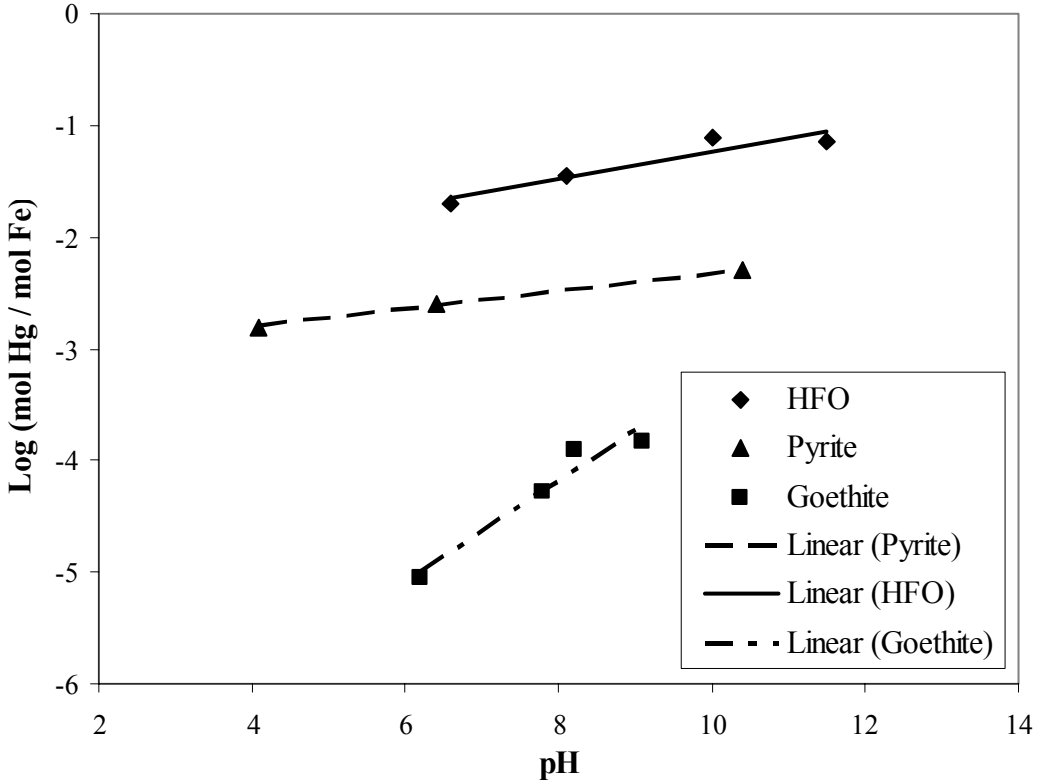

Figure 3.10. Hg(II) Sorption Comparison for Pyrite and Fe Hydroxides.

3.3.2 Column Experiments

Mercury sorption column tests were conducted in order to mimic contaminated groundwater flow and investigate the capabilities of pyrite as a barrier material for Hg(II) during subsurface transport. In order to predict the fate and transport of pollutants in the subsurface, accurate transport parameters must be determined. CXTFIT uses the convection dispersion equation (CDE) as well as the non-linear least squares method to estimate these parameters (Toride et al. 1999). Additionally, CXTFIT can be utilized to produce predictive models that aid in the design of sustainable barrier systems. A 0.1 M KBr tracer test was performed in the sand and pyrite packed column and modeled using CXTFIT in order to determine the dispersion coefficient (D) and Peclet number (P), which were found to be 0.0235 cm^2 min^{-1} and 44, respectively, with an R^2 of 0.98.

Figure 3.11 illustrates the effect of pyrite and dissolved oxygen on Hg(II) sorption. The breakthrough of Hg(II) from the column without pyrite occurred significantly before the breakthroughs from the columns with pyrite, indicating the pyrite was effectively adsorbing the Hg(II). Moreover, it was determined that about 1000 inches of mercury-contaminated infiltration could occur before the pyrite was saturated. Considering the annual average rainfall infiltration in the Southeastern U.S. is about 25 inches (Viessman and Hammer 1998), this pyrite barrier could theoretically sorb mercury at this concentration for up to 40 years.

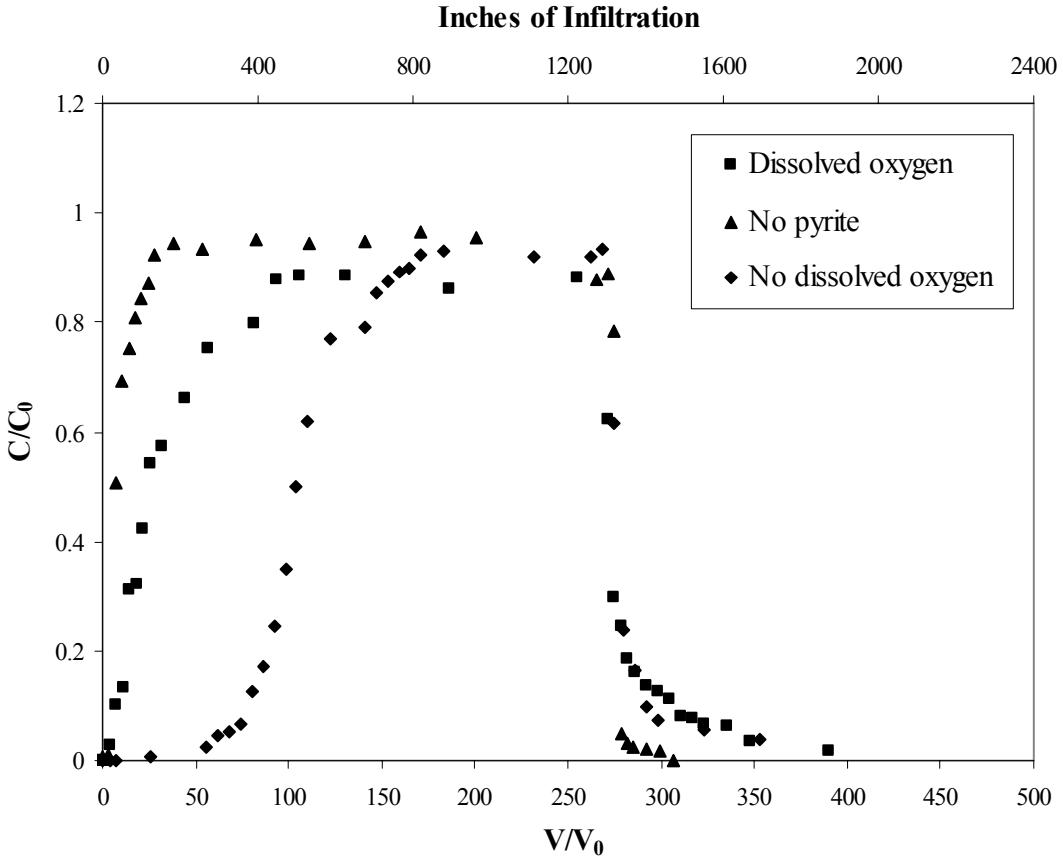

Figure 3.11. Hg(II) transport through column under various conditions. Inlet Hg(II) concentration was 100 μg L^{-1}. Inlet pH was 4.1 ± 0.1. Pyrite in column was 0.0625 g. Ionic strength was 0.1 M NaCl. Flow rate was 0.076 cm min^{-1}.

The total amount of Hg(II) adsorbed onto the pyrite, q (μg g^{-1}), can be determined using the expression

$$q = \frac{\left(C_0 * V_f\right) - \sum C_i V_i\right)}{W}, \tag{3.4}$$

where C_0 is the inlet Hg(II) concentration (100 μg L^{-1}), V_f is the volume of the input pulse, C_i is the Hg(II) effluent concentration at time i, V_i is the effluent volume at time i, and W is the mass of pyrite (0.0625 g). Moreover, the greater the Hg(II) sorption onto pyrite, the greater the retardation will be. The overall retardation factor (R) is calculated using the following equation:

$$R = 1 + \frac{\rho_b}{\theta} K_d \tag{3.5}$$

where ρ_b is the bulk density of the column material, θ is the volumetric water content of the soil, which in this case is the porosity of the soil because the column is always saturated, and K_d is the solid water partition coefficient and is calculated by the following expression

$$K_d = f_p * K_p \tag{3.6}$$

where K_p is the distribution coefficient between pyrite and Hg(II) and f_p is the fraction of pyrite in the column. K_p can be determined by the expression

$$K_p = \frac{q}{C_0}. \tag{3.7}$$

In the column without pyrite, 0.5 ug Hg(II) g^{-1} remained on the sand, showing that a negligible amount of Hg(II) sorbed onto the sand. Additionally, during desorption with 0.1 M NaCl, all of the Hg(II) was removed. R in the column without dissolved oxygen was determined to be about 108, while R in the column with dissolved oxygen was

determined to be about 49, showing that dissolved oxygen plays a major role in Hg(II) adsorption onto pyrite. When dissolved oxygen was absent, 260 μg Hg(II) g^{-1} pyrite was sorbed, while only 8% (21.7 μg Hg(II) g^{-1}) was desorbed by the 0.1 M NaCl solution. In the presence of dissolved oxygen, 120 μg Hg(II) g^{-1} pyrite was sorbed, and about 24% (28.5 μg Hg(II) g^{-1}) of the Hg(II) was desorbed by the 0.1 M NaCl solution. Sorption increased two-fold in the absence of dissolved oxygen, revealing that dissolved oxygen can inhibit Hg(II) sorption onto pyrite. In addition, iron hydroxides, such as goethite, would most likely form from pyrite oxidation in the column with dissolved oxygen. Goethite has been shown to adsorb Hg(II) only at basic pH and have a lower sorption capacity for Hg(II) than pyrite (Bonnissel-Gissinger et al. 1999). Furthermore, the amount of Hg(II) released from the pyrite is less than that retained on the pyrite under both aerobic and anaerobic conditions, revealing that the majority of the Hg(II) is not readily desorbed, and that the adsorption – desorption processes is not reversible or it exhibits hysteresis. This is most likely due to the strong binding of Hg(II) to high affinity S sites or mercury sulfide solid formation.

Pyrite oxidation has been known to cause solutions to become acidic and release Fe, such as with acid mine drainage (AMD) (Blodau 2006). The effluent pH in the columns was monitored, and the pH values did not drop below the influent pH of 4.1. Furthermore, effluent Fe concentrations were measured and determined to be below the detection limit (1ppm); however, this was possibly due to the small quantity of pyrite that was initially in the column (0.0625 g). In addition, the presence of Hg(II) may have limited pyrite oxidation, as observed by Behra (2001).

In order to determine whether equilibrium was reached in the column, the infiltration rate was varied. Figures 3.12 and 3.13 illustrate the infiltration rate dependence of Hg(II) sorption onto pyrite in the columns. Increasing the infiltration rate from 0.076 cm min^{-1} to 0.255 cm min^{-1} (decreasing the residence time from about 24 minutes to about 7 minutes) significantly increased Hg(II) mobility. This difference in adsorption with residence time provides evidence that Hg(II) removal by pyrite is kinetically controlled in the column.

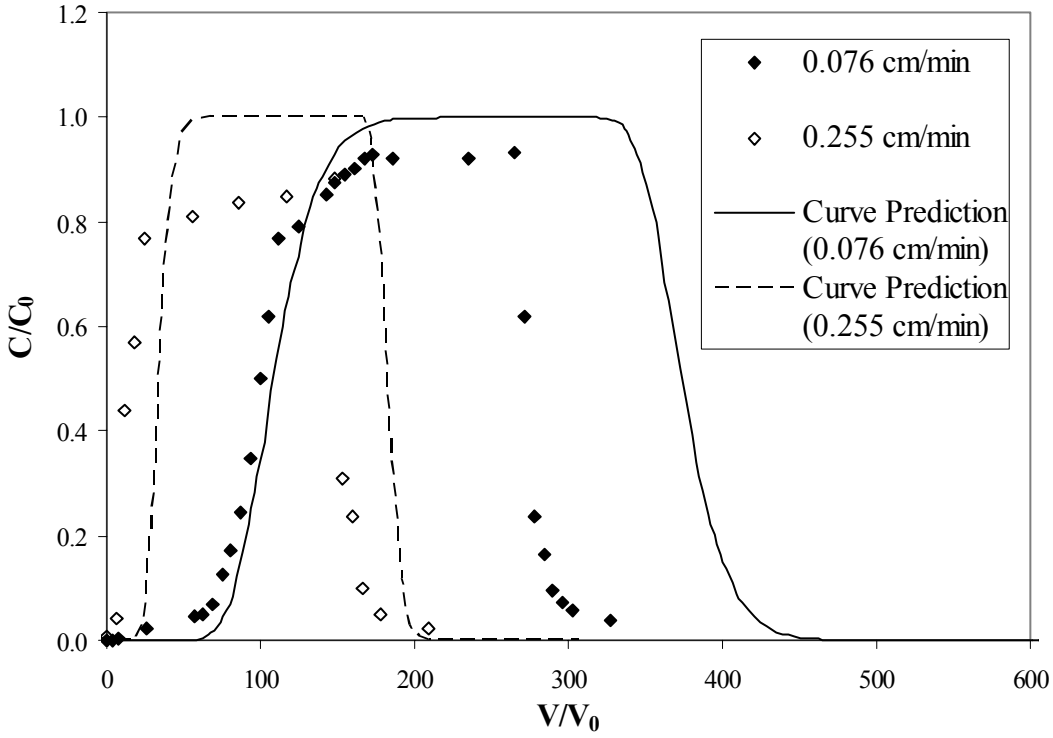

Figure 3.12. Hg(II) transport through column at differing infiltration rates and predictions from kinetic test using CXTFIT. Inlet Hg(II) concentration was 100 μg L^{-1}. Inlet pH was 4.1 ± 0.1. Pyrite in column was 0.0625 g. Ionic strength was 0.1 M NaCl.

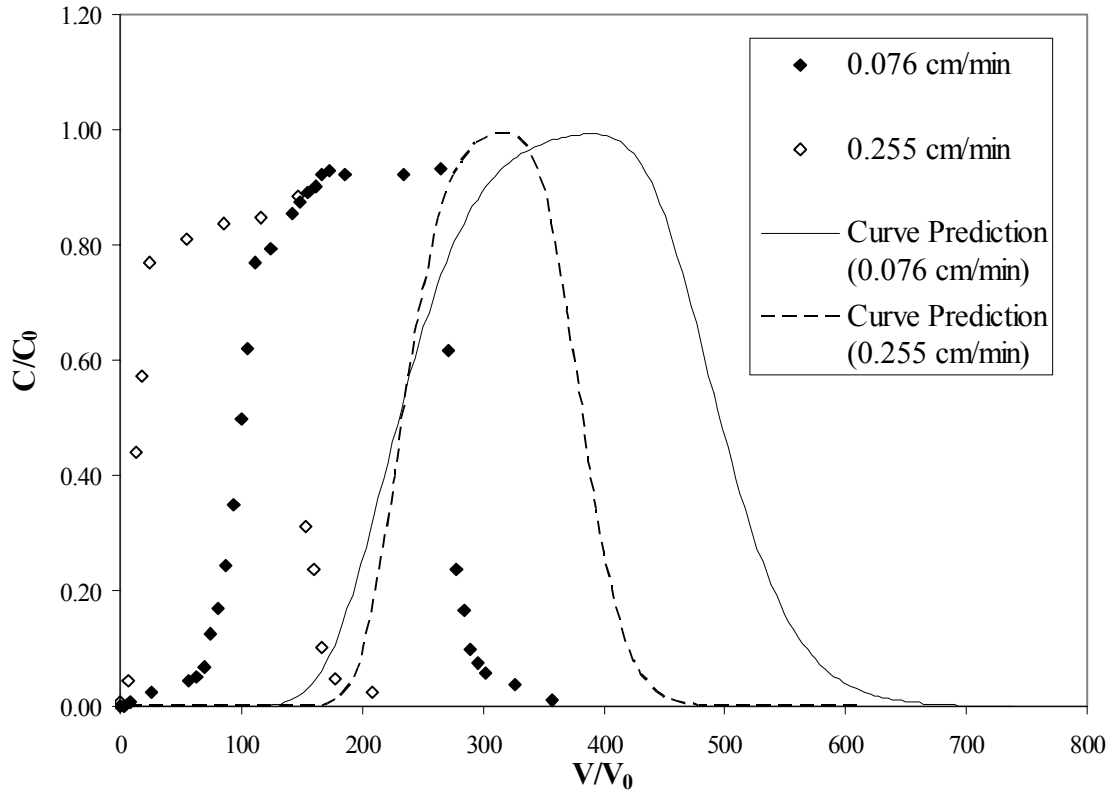

Figure 3.13. Hg(II) transport through column at differing infiltration rates and predictions from isotherm test using CXTFIT. Inlet Hg(II) concentration was 100 µg L^{-1}. Inlet pH was 4.1 ± 0.1. Pyrite in column was 0.0625 g. Ionic strength was 0.1 M NaCl.

CXTFIT was utilized to predict local linear equilibrium (LLE) BTCs in the columns. The BTCs were predicted using K_d values from both kinetic (Fig 3.12) and isotherm results (Fig 3.13). The K_d values determined from the column tests corresponded closely to those observed in the batch kinetic tests at similar reaction time and pH. The K_d was calculated to be 2520 mL g^{-1} at the point when the input pulse was turned off in the slower column (about 48 hours of contact time). The K_d for the kinetic test after two days was determined to be about 2580 mL g^{-1}. Similarly, in the faster column, K_d was calculated to be 765 mL g^{-1} at the point when the input pulse was turned off (18 hours of contact time), while the K_d was determined to be about 795 mL g^{-1} after about 18 hours in the batch kinetic test. The models predicted sorption fairly well. However, the total amount of Hg(II) recovered was lower than predicted based on the models, revealing that the model does not consider irreversible sorption or slow desorption.

For the isotherm test at pH 4 and a C of 100 μg L^{-1}, the K_d value was determined to be about 5500 mL g^{-1}, which is significantly higher than that found in the kinetic and column tests, further demonstrating sorption nonequilibrium. The model predicts adsorption better in the slower column because it is nearer to equilibrium than the faster column. Furthermore, the shapes of the BTCs were asymmetric, which is indicative of rate-limited and/or non-linear adsorption (Brusseau 1998), both of which were observed in kinetic and equilibrium batch experiments. Moreover, it was found that as the infiltration rate decreased, the relative concentration neared 1.0. Had equilibrium been attained, the relative concentration would have reached 1.0, as illustrated by the equilibrium model predictions.

3.4 Conclusions

The results of this study reveal significant findings regarding the adsorption and subsurface transport of Hg(II) in the presence of quartz sand and pyrite. Hg(II) sorption and removal rate increased with increasing pH, most likely due to increased hydrolysis, pH dependent surface charge, and a greater amount of high affinity sorption sites. The adsorption rate exhibited a biphasic pattern, which is characterized by a rapid initial uptake followed by a period of slower uptake. Furthermore, Langmuir, Temkin, and Linear isotherms were able to fit the sorption data at acidic, neutral, and basic pH, respectively. In the column experiments, pyrite effectively adsorbed Hg(II), demonstrating its potential as a barrier material. Dissolved oxygen hindered sorption of Hg(II) onto pyrite, most likely due to the formation of iron (hydr)oxides which are less efficient adsorbents for Hg(II) than pyrite at low pH. Additionally, increasing the infiltration rate shifted the BTC leftward and increased the mobility of Hg(II) in the column. Due to nonequilibrium, the LLE models over predicted the BTCs; however, the presence of an irreversible fraction of Hg(II) on the pyrite acted to counteract the increased mobility. Moreover, the nonlinearity of the column BTCs is consistent with the sorption nonlinearity determined from the equilibrium isotherm at similar pH.

CHAPTER FOUR

INVESTIGATION OF HG(II) REMOVAL BY IRON SULFIDE

4.1 Introduction

Mercury is a pervasive contaminant that has caused environmental and health problems throughout the world. Numerous industries including coal-fired power plants and chlor-alkali plants have discharged mercury pollution into the environment (Matlock et al. 2003; Yudovich and Ketris 2005). The unique physical properties of mercury including high specific gravity, volatility, and electrical conductivity have made it attractive to industries, but have also made it difficult to attain and recover (USEPA 1997). Most of the mercury contamination is in the form of Hg^0, which has a high solubility and easily oxidizes to soluble inorganic Hg(II) (Morel et al. 1998). This soluble inorganic Hg(II) becomes a problem when it is methylated to form methyl mercury (MeHg). MeHg bioaccumulates up the aquatic food chain, causing mercury concentrations in predatory fish to be up to one million times higher than in the water column. Consequently, consumption of contaminated fish can cause severe neurotoxic effects to both humans a wildlife (Stein et al. 1996). Therefore, the United States Environmental Protection Agency (US EPA) has identified mercury as on of its twelve persistent bioaccumulative and toxic (PBT) chemicals.

In order to prevent methylation, mercury must be removed from or immobilized at sites before it can enter surface waters. Excavation and thermal treatment has often been employed to remove contaminated soils from these sites. However, this is often not economically feasible and can result in mercury air emissions. Furthermore, Hg^0 in soils exists as a dense non-aqueous phase liquid (DNAPL) with a high surface tension, and disturbing the soils often causes the contamination to spread (Piao and Bishop 2006). An alternative method is in situ immobilization of mercury using sulfide minerals.

Mercury can undergo complex physical and chemical transformations, which determine its reactivity, mobility, and bioaccumulation. Research has shown that sulfides play a major role in controlling the fate and transport of mercury. FeS(s) has been shown to readily exchange Fe^{2+} with Hg^{2+} to form HgS(s) (Morse and Luther 1999; Jeong 2005; Svensson et al. 2006a). HgS(s) is relatively insoluble and less volatile than other forms of mercury, and thus potentially less harmful (Willet 1992; Barnett et al. 2001). It has also been suggested that HgS(s), due to its low solubility, may limit mercury cycling though the environment (Krabbenhoft and Babiarz 1992; Barnett et al. 2001). Thus, the formation of HgS(s) from mercury and sulfide interactions in water, soil, and sediments provides evidence that mercury pollution can be abated.

In this study, preliminary sorption experiments were carried out using FeS(s), pyrite, and pyrrhotite in order to determine the most efficient iron-sulfide mineral for Hg(II) removal. Further batch experiments were conducted to investigate the kinetic and thermodynamic parameters involved in Hg(II) immobilization by FeS(s). This was achieved by observing sorption changes due to variation in pH, FeS(s)/Hg(II) molar ratios, and reaction time. In addition, solid phase characterization was achieved using

X-ray diffraction (XRD). These parameters and characterizations will aid in understanding the fate and transport of mercury in the environment. Furthermore, this research will promote a further understanding and predictive capability for mercury immobilization using sulfide minerals.

4.2 Materials & Methods

4.2.1 Iron Sulfide

The iron(II) sulfide (99.9% metals basis, < 100 mesh) in this study was obtained from Alfa Aesar. XRD results indicated both troilite (FeS) and pyrrhotite ($Fe_{1-x}S_x$) were present. The specific surface area of the powder was estimated to be 0.87 $m^2\ g^{-1}$ (Kr BET at 77 K). The iron sulfide was washed with 0.01 M HCl to remove oxidation products and stored under anaerobic conditions in an anaerobic chamber until use.

4.2.2 Pyrite and Pyrrhotite

The pyrite and pyrrhotite used in this study were obtained from Wards Science Co. The rocks were crushed, pulverized with a mortar and pestle, and then sieved to < 250 microns. The powders were washed with 0.01 M HCl to remove oxidation products and stored under anaerobic conditions until use. Removal of oxidation products and the purity of the minerals were confirmed by XRD.

4.2.3 Batch Experiments

Due to the high reactivity of iron sulfide toward molecular oxygen, anaerobic conditions were maintained by conducting experiments inside a glove box under $N_2(g)$

atmosphere. All solutions were prepared using deoxygenated Milli-Q water by purging with N_2(g). Batch experiments were performed in 45 mL Teflon vials. Each vial contained 0.5 or 2 g L^{-1} iron sulfide. Stock solutions of Hg(II) were prepared using a standard solution of $Hg(NO_3)_2$ with a concentration of 1 g L^{-1} and diluted with deoxygenated Milli-Q water, resulting in initial Hg(II) concentrations ranging from 1.6 to 100 mg L^{-1}. Adjustments in pH were made using N_2 sparged 0.05 or 0.5 M NaOH or HCl. Reaction times were 24 hours except in the kinetic experiments. All suspensions were prepared in a constant ionic strength background matrix of 0.1 M NaCl because Hg(II) forms very strong associations with chloride ions, which helped to stabilize the Hg(II) in solution. Samples were centrifuged at 2500 g for 25 minutes at 25ºC and filtered through a 0.45 acrodisk syringe filter membrane to separate solids from the liquid. Sub-samples of the filtrate were taken to measure the pH of each sample.

4.2.4 Analytical Methods

Mercury analysis was conducted by Cold Vapor Atomic Absorption Spectrophotometry (CVAAS-USEPA Methods 7470A and 7471A). Mercury sample preparation, preservation, and analysis were conducted similar to these two procedures and those described in EPA Method 1631. Prior to analysis, all samples are preserved and oxidized with 1% BrCl, followed by 1% hydroxylamine hydrochloride to destroy the unreacted BrCl. Spikes, blanks, and duplicates were run to estimate process error and quantify possible losses to containers. Teflon containers were used to minimize sorption to container walls.

Powder XRD was performed on a Rigaku Miniflex Diffractometer using Cu-Kα radiation (30 kV, 15 mA). Diffraction data were collected in the range of $3^o < 2\theta < 90^o$ at a rate of 0.10^o (2θ) min^{-1}. For detailed structure information, the results were analyzed using JADE (Version 6.0), a software tool for XRD powder pattern processing.

4.3 Results & Discussion

Preliminary batch experiments were carried out using several iron sulfide minerals at various pH values in order to compare their effectiveness for Hg(II) removal from solution (Fig. 4.1). Initial Hg(II) and iron sulfide concentrations were 1.6 mg L^{-1} and 2 g L^{-1}, respectively. It was observed that the FeS(s) resulted in the highest Hg(II) removal throughout the pH range, followed by pyrite and then pyrrhotite (linear trendlines were added for clarity). Thus, further batch tests were conducted using FeS(s).

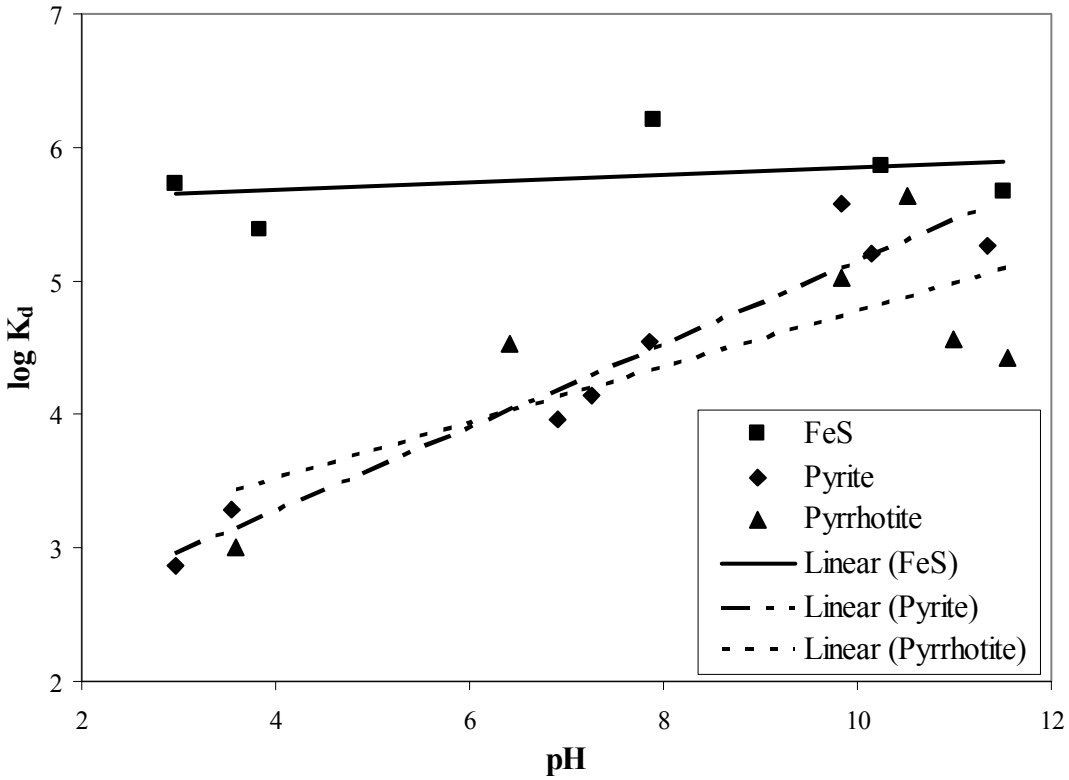

Figure 4.1. Comparison of Hg(II) sorption for various iron sulfide minerals. Initial Hg(II) and pyrite concentrations were 1.6 mg L^{-1} and 2 g L^{-1}, respectively. Reaction time was 24 hours. Ionic strength was 0.1 M NaCl. pH was adjusted using 0.05 M HCl or NaOH.

Batch tests were conducted in which the pH was varied from 2 to 12 in order to determine the effect of pH on Hg(II) sorption to the FeS(s). Figures 4.2 – 4.5 show Hg(II) removal at molar ratios of Hg(II) to FeS(s) ranging from 4.4×10^{-4} to 8.8×10^{-2}. The higher molar ratios simulate environments with high mercury contamination such as industrial waste sites and mine tailings, while the lower molar ratios imitate sulfide-rich environments such as estuaries and wetlands. The lower molar ratios of Hg(II) / FeS(s) seem to be more ideal for efficient Hg(II) removal, as would be expected.

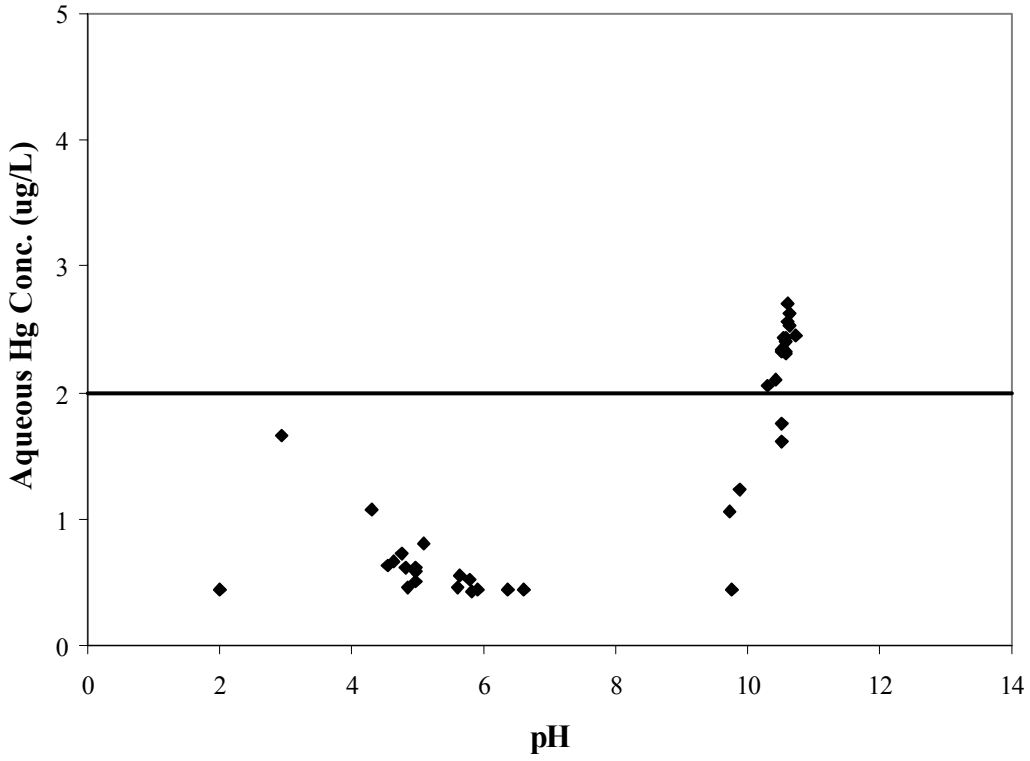

Figure 4.2. Sorption onto FeS(s) as a Function of pH, $Hg(II)_0$ / FeS(s) = 4.4 x 10^{-4}. Initial Hg(II) and pyrite concentrations were 2 mg L^{-1} and 2 g L^{-1}, respectively. Reaction time was 24 hours. Ionic strength was 0.1 M NaCl. pH was adjusted using 0.05 M HCl or NaOH. Bold line is EPA MCL (2ppb).

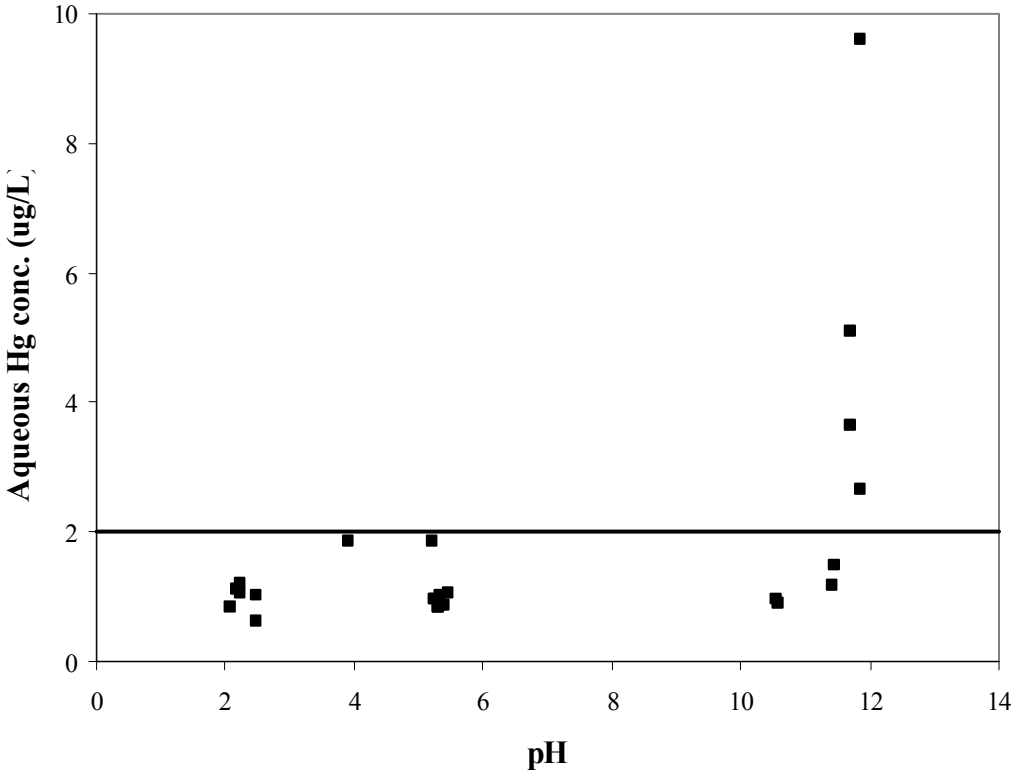

Figure 4.3. Sorption onto FeS(s) as a Function of pH, $Hg(II)_0$ / FeS(s) = 4.4 x 10^{-3}. Initial Hg(II) and pyrite concentrations were 20 mg L^{-1} and 2 g L^{-1}, respectively. Reaction time was 24 hours. Ionic strength was 0.1 M NaCl. pH was adjusted using 0.05 M HCl or NaOH. Bold line is EPA MCL (2ppb).

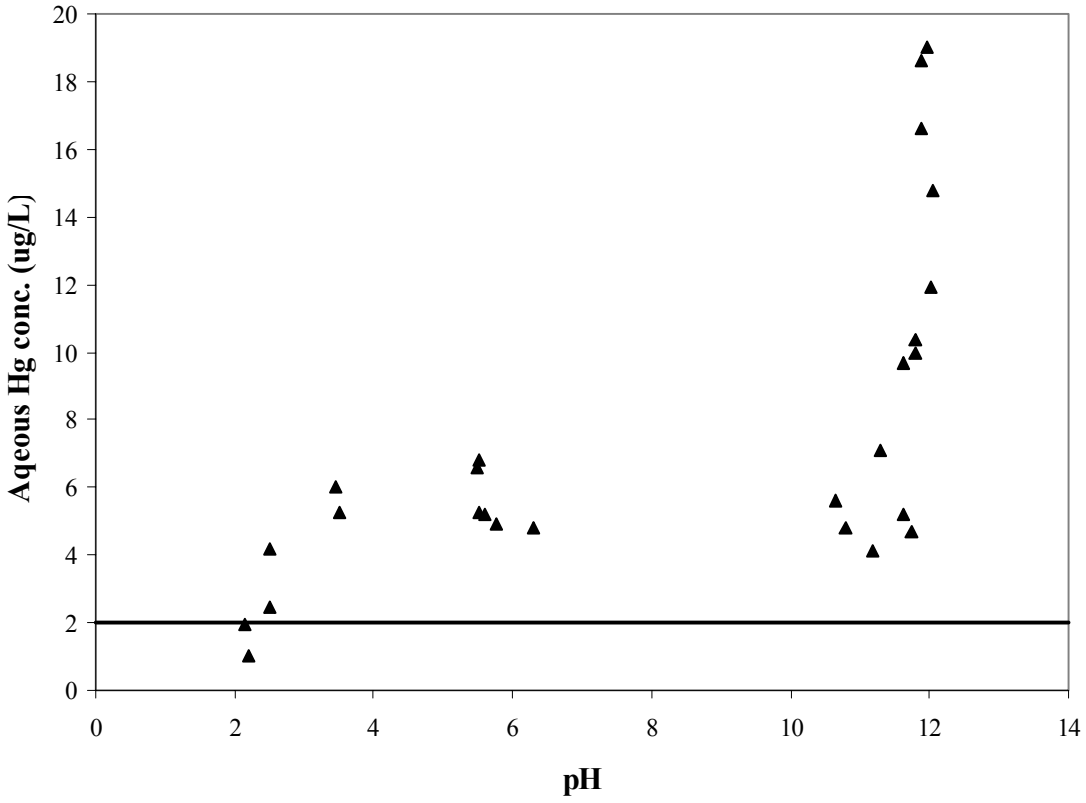

Figure 4.4. Sorption onto FeS(s) as a Function of pH, $Hg(II)_0$ / FeS(s) = 2.2 x 10^{-2}. Initial Hg(II) and pyrite concentrations were 100 mg L^{-1} and 2 g L^{-1}, respectively. Reaction time was 24 hours. Ionic strength was 0.1 M NaCl. pH was adjusted using 0.05 M HCl or NaOH. Bold line is EPA MCL (2ppb).

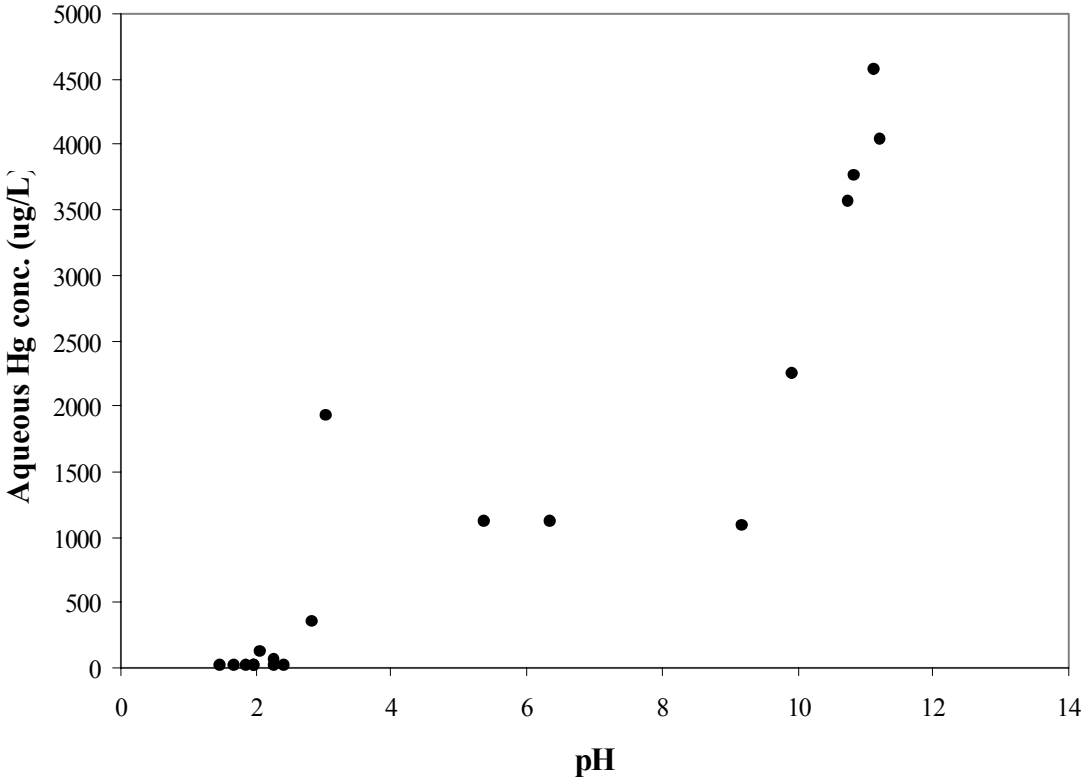

Figure 4.5. Sorption onto FeS(s) as a Function of pH, $Hg(II)_0$ / FeS(s) = 8.8 x 10^{-2}. Initial Hg(II) and pyrite concentrations were 100 mg L^{-1} and 0.5 g L^{-1}, respectively. Ionic strength was 0.1 M NaCl. pH was adjusted using 0.05 M HCl or NaOH.

Generally, for cation adsorption removal increases with increasing pH, which in the case of Hg(II) and pyrite is explained by the notion that hydrolysis of Hg(II) is required for adsorption to take place (Jenne 1998; Behra et al. 2001). This is not the pattern found here however, indicating that a more complicated chemical reaction is occurring. Nevertheless, a similar adsorption pattern was observed for the all molar ratios (Fig 4.2-4.5). It was found that at acidic pH (between 2 and 4), Hg(II) removal decreased with increasing pH. Then, at very high pH (between 10 and 12), Hg(II) removal decreased again with increasing pH. A similar adsorption pattern was found by Piao and Bishop (2006). Data points between pH 6 and 10 were difficult to obtain due to the solution pH instability in this range. A buffer was not used in order to prevent adsorption competition effects. However, it appears that the aqueous phase equilibrium Hg(II) concentrations would remain relatively constant between that pH range.

For initial Hg(II) and FeS(s) concentrations of 2 mg L^{-1} and 2 g L^{-1}, respectively ($(Hg(II)_0$ / FeS(s) = 4.4 x 10^{-4}), over 99.9% of the Hg(II) is removed from solution and all aqueous phase concentrations below pH 10.5 were below U.S. EPA standards (<2 ppb) (USEPA 2006) (Fig 4.2). For initial Hg(II) and FeS(s) concentrations of 20 mg L^{-1} and 2 g L^{-1}, respectively ($(Hg(II)_0$ / FeS(s) = 4.4 x 10^{-3}), over 99.9% of the Hg(II) is removed from solution and all aqueous phase concentrations below pH 11.5 were below EPA standards (Fig 4.3). For initial Hg(II) and FeS(s) concentrations of 100 mg L^{-1} and 2 g L^{-1}, respectively ($(Hg(II)_0$ / FeS(s) = 2.2 x 10^{-2}), over 99.9% of the Hg(II) is removed from solution along the pH range, but only below pH 2.5 is the concentration below EPA standards (Fig 4.4). For initial Hg(II) and FeS(s) concentrations of 100 mg L^{-1} and 0.5 g L^{-1}, respectively ($(Hg(II)_0$ / FeS(s) = 8.8 x 10^{-2}), over 95% of the Hg(II) is removed from

solution along the pH range, but the Hg(II) concentrations never reach below EPA standards (Fig 4.5). Lowering the molar ratio only by a factor of 4 caused a significant increase in aqueous phase equilibrium Hg(II) concentrations (> 2 orders of magnitude). Thus, to ensure efficient Hg(II) removal at contaminated sites, FeS(s) should be provided at molar quantities much higher than the total Hg to be treated. It has been found, however, that the solubility of HgS(s) can be increased in the presence of high dissolved sulfide concentrations (Paquette and Helz 1997). HgS(s) formation is generally desired over adsorption in terms of mobility. Nonetheless, Jeong (2005) found that neither adsorbed nor coprecipitated Hg was readily desorbed from synthesized mackinawite, FeS(s), by strong ligands. It was also found that when $Hg(II)_0$/FeS(s) exceeded 1, the sulfide concentration was no longer sufficient for coprecipitation, and chloride salts (Hg_2Cl_2 and $HgCl_2$•3HgO) became responsible for Hg(II) removal. Additionally, Jeong (2005) calculated the maximum sorption capacity of Hg(II) to FeS(s) to be 0.23 mmol g^{-1} (46 mg g^{-1}) at pH 5.5-6.0. This was the exact sorption capacity calculated at the molar ratio $Hg(II)_0$ / FeS(s) = 2.2 x 10^{-2} in the same pH range.

Calculations of the solubility of 2 g L^{-1} FeS(s) in a system containing 2 mg L^{-1} Hg(II) at 0.1 M NaCl were made using VisualMINTEQ. The results revealed that thermodynamically, below pH 4, all of the FeS(s) should have dissolved in solution, while above pH 4, little to no FeS(s) was shown to dissolve. However, FeS(s) dissolution was not observed visually at any pH. Moreover, the $Hg(HS)_2$(aq) species was found to dominate in solution at acidic pH, and HgS_2^{-2} was the primary Hg(II) species in solution at basic pH. HgS(s) was found to form thermodynamically to the same extent at all pH

values. Additionally, VisualMINTEQ showed the formation of $Fe(OH)_2(s)$ to occur above pH 8, and its concentration increased with pH.

Batch kinetic experiments revealed the rates of Hg(II) removal from solution by FeS(s). These experiments were performed at an initial Hg(II) concentration of 2 mg L^{-1} at pH 4.8, 6.7, and 10.3 (± 0.2) in order to determine equilibrium attainment times at acidic, neutral, and basic pH values. Figure 4.7 illustrates the increase in Hg(II) removal rate with pH. The removal rate conveys a biphasic pattern in which initially Hg(II) uptake is rapid, followed by a slower removal rate, which has been attributed to the high affinity sites initially being filled rapidly, followed by the lower affinity sites being filled more slowly (Axe and Anderson 1995). At acidic pH, more than 99% Hg(II) removal is achieved in about 12 hours. Equivalent removal is achieved in 4 hours at neutral pH. While at basic pH, over 99% of the Hg(II) is removed from solution in only 2 hours. This difference in removal time with pH could possibly be explained by the concept that an Fe hydroxide layer forms as pH increases, which can adsorb Hg(II) at basic pH, resulting in two types of adsorption sites (Axe and Anderson 1998; Bonnissel-Gissinger et al. 1998). The calculations from VisualMINTEQ also reveal the formation of $Fe(OH)_2$. However, this conclusion does not completely correspond to the pH edge results, which demonstrate lower sorption at very basic pH. The reaction rate at pH 10.3 may be faster due to simpler reaction pathways, i.e. adsorption, while at pH 4.8 and 6.7, HgS(s) formation is most likely occurring, which is a slower process but results in greater Hg(II) removal.

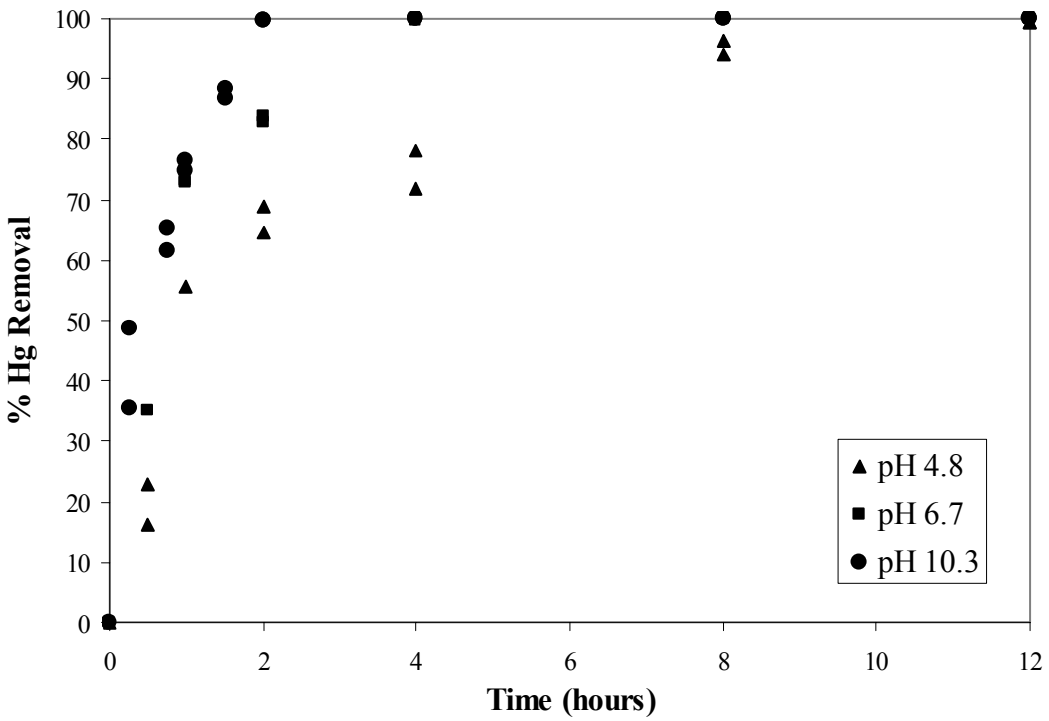

Figure 4.6. Hg(II) sorption onto FeS(s) as a function of time. Initial Hg(II) and FeS(s) concentrations were 2 mg L^{-1} and 2 g L^{-1}, respectively. Ionic strength was 0.1 M NaCl. Experiments were carried out at pH 4.8, 6.7, and 10.3 ± 0.2.

XRD analysis was conducted on acidic, neutral, and basic Hg(II)–sorbed FeS(s) samples from the 2 mg L^{-1} pH edge tests. No solid formations were found on the acidic or basic samples. Metacinnabar (β-HgS) was found on the neutral samples (pH 6.5 ± 0.2), indicating a high HgS(s) concentration on these samples (Fig 4.8a). Fig 4.8b shows the XRD results of the FeS(s) alone, while 4.8a shows the FeS(s) with HgS(s) formation. The main HgS(s) peaks occur at theta values of 26.5, 43.9 and 52.0, while smaller peaks appear around 31.4, 54.4, 70.2, 72.2, 81.6, and 86.6. Moreover, Jeong (2005) found that β-HgS was present in all Hg(II)-sorbed FeS(s) samples ($Hg(II)_0$ / FeS(s) <1 and various pH) using extended X-ray adsorption fine structure (EXAFS).

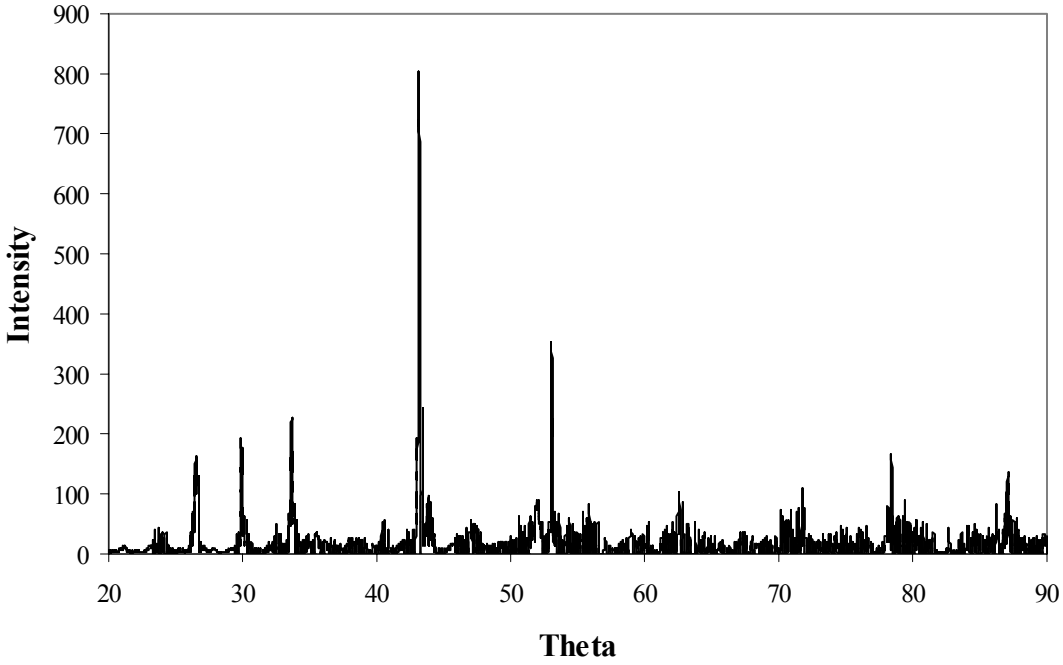

Figure 4.7a. XRD results for Hg(II) sorbed FeS(s). Initial Hg(II) and FeS(s) concentrations were 2 mg L^{-1} and 2 g L^{-1}, respectively. Ionic strength was 0.1 M NaCl. Experiment was carried out at pH 6.7 ± 0.2 (no adjustments in pH were made).

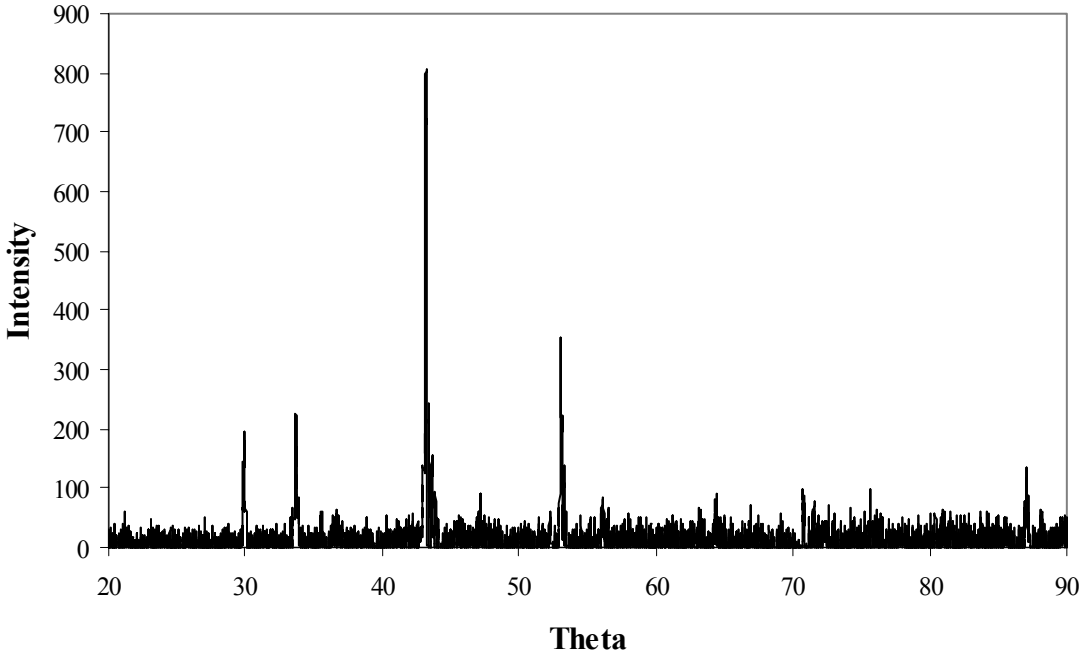

Figure 4.7b. XRD results for FeS(s).

4.4 Conclusions

This study revealed effectiveness of FeS(s) for the removal of Hg(II) from aqueous solution. The experimental results demonstrated that the chemical interactions between Hg(II) and FeS(s) were highly dependent on environmental variables including pH, $Hg(II)_0$/FeS(s) molar ratio, and reaction time. The pH edge experiments showed that the most efficient Hg(II) removal occurred at very acidic pH and neutral pH. Hg(II) sorption was found to increase with reaction time, most likely due to Fe hydroxide formation at basic pH and HgS(s) formation at neutral pH. Additionally, the adsorption rate exhibited a biphasic pattern, which may be attributed to the high affinity sites initially being filled rapidly, followed by the lower affinity sites being filled more slowly. Furthermore, XRD indicated the presence of metacinnabar in a sample with low initial Hg(II) concentration and neutral pH. The formation of HgS(s) in this study confirms the potential use of FeS(s) as a barrier material for subsurface mercury remediation.

CHAPTER FIVE
CONCLUSIONS AND RECOMMENDATIONS

5.1 Conclusions

In this research, iron sulfide minerals were tested for their ability to immobilize Hg(II). It was determined that both pyrite and FeS(s) can effectively remove Hg(II) from aqueous solution. For pyrite, the mechanism of removal was most likely adsorption, possibly followed by solid formation. Moreover, an Fe hydroxide layer is postulated to form on iron sulfides at basic pH, resulting in additional adsorption sites. Therefore, faster sorption is achieved at high pH. Furthermore, the dominant mercury species at high pH is $Hg(OH)_2$, which has been suggested to have a greater affinity for iron sulfides than mercury-chloride species, which dominate at low pH. Column studies demonstrated the potential for the use of pyrite as a barrier material to intercept mercury-contaminated subsurface groundwater flow, such as in a permeable reactive barrier. However, the presence of dissolved oxygen reduced Hg(II) sorption onto pyrite, illustrating that anoxic conditions are best suited for its use.

The mechanism of Hg(II) removal by FeS(s) was most likely HgS(s) formation at neutral pH and adsorption at basic pH. As a result, the capability of FeS(s) to remove Hg(II) at high concentrations was better than that of pyrite. Thus, FeS(s) could potentially serve as a better barrier material than pyrite for the remediation of mercury.

5.2 Recommendations

In order to determine the potential of FeS(s) as a barrier material for Hg(II), further column studies should be conducted using this mineral. FeS(s) should be tested under both aerobic and anaerobic conditions. Additionally, because it has a higher capacity for Hg(II) removal than pyrite, a much higher input Hg(II) concentration should be utilized.

Mercury contamination is most often released as Hg^0, and recent studies have detected traces of HgS(s) in samples containing Hg^0 and pyrite (Navarro et al. 2006; Svensson et al. 2006a); therefore, further experiments should be conducted using these materials.

The mechanisms responsible for immobilization of Hg(II) using these iron sulfide minerals has been probed using X-ray adsorption fine structure (XAFS) at Argonne National Laboratory. These results should be analyzed and compiled to provide further evidence for the immobilization mechanisms proposed in this research.

REFERENCES

Amyot, M., F. M. M. Morel and P. A. Ariya (2005). "Dark oxidation of dissolved and liquid elemental mercury in aquatic environments." Environmental Science & Technology **39**(1): 110-114.

Axe, L. and P. R. Anderson (1995). "Sr Diffusion and Reaction within Fe Oxides - Evaluation of the Rate-Limiting Mechanism for Sorption." Journal of Colloid and Interface Science **175**(1): 157-165.

Axe, L. and P. R. Anderson (1998). Intraparticle Diffusion of Metal Contaminants in Amorphous Oxide Minerals. Adsorption of Metals by Geomedia. E. A. Jenne, Academic Press. **8:** 193-205.

Barnett, M. O., L. A. Harris, R. R. Turner, R. J. Stevenson, T. J. Henson, R. C. Melton and D. P. Hoffman (1997). "Formation of mercuric sulfide in soil." Environmental Science & Technology **31**(11): 3037-3043.

Barnett, M. O., R. R. Turner and P. C. Singer (2001). "Oxidative dissolution of metacinnabar (beta-HgS) by dissolved oxygen." Applied Geochemistry **16**(13): 1499-1512.

Behra, P., P. Bonnissel-Gissinger, M. Alnot, R. Revel and J. J. Ehrhardt (2001). "XPS and XAS study of the sorption of Hg(II) onto pyrite." Langmuir **17**(13): 3970-3979.

Benoit, J. M., C. C. Gilmour, A. Heyes, R. P. Mason and C. L. Miller (2003). Geochemical and biological controls over methylmercury production and

degradation in aquatic ecosystems. Biogeochemistry of Environmentally Important Trace Elements. **835:** 262-297.

Blodau, C. (2006). "A review of acidity generation and consumption in acidic coal mine lakes and their watersheds." Science of the Total Environment **369**(1-3): 307-332.

Bonnissel-Gissinger, P., M. Alnot, J. J. Ehrhardt and P. Behra (1998). "Surface oxidation of pyrite as a function of pH." Environmental Science & Technology **32**(19): 2839-2845.

Bonnissel-Gissinger, P., M. Alnot, J.-P. Lickes, J.-J. Ehrhardt and P. Behra (1999). "Modeling the Adsorption of Mercury(II) on (Hydr)oxides II: [alpha]-FeOOH (Goethite) and Amorphous Silica." Journal of Colloid and Interface Science **215**(2): 313-322.

Brown, J. R., G. M. Bancroft, W. S. Fyfe and R. A. N. McLean (1979). "Mercury Removal from Water by Iron Sulfide Minerals - Electron-Spectroscopy for Chemical-Analysis (Esca) Study." Environmental Science & Technology **13**(9): 1142-1144.

Brusseau, M. L. (1998). Impact of chemical and biochemical reactions on transport of environmental pollutants in porous media. Soil Chemistry and Ecosystem Health. P. M. Huang, D. C. Adriano, T. J. Logan and R. T. Checkai. Madison, WI., SSSA Spec. Publ. 52**:** 173-189.

Charnock, J. M., L. N. Moyes, R. A. D. Pattrick, J. F. W. Mosselmans, D. J. Vaughan and F. R. Livens (2003). "The structural evolution of mercury sulfide precipitate: an XAS and XRD study." American Mineralogist **88**(8-9): 1197-1203.

Ebadian, M. A. (2001). Mercury Contaminated Material Decontamination Methods: Investigation and Assessment. Miami, Florida International University**:** 61.

Ehrhardt, J. J., P. Behra, P. Bonnissel-Gissinger and M. Alnot (2000). "XPS study of the sorption of Hg(II) onto pyrite FeS2." Surface and Interface Analysis **30**(1): 269-272.

Gustin, M. S., H. Biester and C. S. Kim (2002). "Investigation of the light-enhanced emission of mercury from naturally enriched substrates." Atmospheric Environment **36**(20): 3241-3254.

Han, Y., H. M. Kingston, H. M. Boylan, G. M. M. Rahman, S. Shah, R. C. Richter, D. D. Link and S. Bhandari (2003). "Speciation of mercury in soil and sediment by selective solvent and acid extraction." Analytical and Bioanalytical Chemistry **375**(5): 428-436.

Ho, Y. S., J. F. Porter and G. McKay (2002). "Equilibrium isotherm studies for the sorption of divalent metal ions onto peat: Copper, nickel and lead single component systems." Water Air and Soil Pollution **141**(1-4): 1-33.

Huerta-Diaz, M. A. and J. W. Morse (1992). "Pyritization of trace metals in anoxic marine sediments." Geochimica et Cosmochimica Acta **56**(7): 2681-2702.

Hyland, M. M., G. E. Jean and G. M. Bancroft (1990). "Xps and Aes Studies of Hg(Ii) Sorption and Desorption Reactions on Sulfide Minerals." Geochimica Et Cosmochimica Acta **54**(7): 1957-1967.

James, R. O. and M. G. MacNaughton (1977). "The adsorption of aqueous heavy metals on inorganic minerals." Geochimica et Cosmochimica Acta **41**(11): 1549-1555.

Jay, J. A., F. M. M. Morel and H. F. Hemond (2000). "Mercury speciation in the presence of polysulfides." Environmental Science & Technology **34**(11): 2196-2200.

Jean, G. E. and G. M. Bancroft (1986). "Heavy metal adsorption by sulphide mineral surfaces." Geochimica et Cosmochimica Acta **50**(7): 1455-1463.

Jenne, E. A. (1998). Adsorption of Metals by Geomedia, Academic Press.

Jeong, H. Y. (2005). Removal of Heavy Metals and Reductive Dechlorination of Chlorinated Organic Pollutants by Nanosized FeS. Civil and Environmental Engineering. Ann Arbor, University of Michigan. **Ph.D.:** 217.

King, J. K., S. M. Harmon, T. T. Fu and J. B. Gladden (2002). "Mercury removal, methylmercury formation, and sulfate-reducing bacteria profiles in wetland mesocosms." Chemosphere **46**(6): 859-870.

King, J. K., J. E. Kostka, M. E. Frischer and F. M. Saunders (2000). "Sulfate-reducing bacteria methylate mercury at variable rates in pure culture and in marine sediments." Applied and Environmental Microbiology **66**(6): 2430-2437.

Krabbenhoft, D. P. and C. L. Babiarz (1992). "The Role of Groundwater Transport in Aquatic Mercury Cycling." Water Resources Research **28**(12): 3119-3128.

Matlock, M. M., B. S. Howerton and D. A. Atwood (2003). "Irreversible binding of mercury from contaminated soil." Advances in Environmental Research **7**(2): 347-352.

Morel, F.-M., and Hering, JG. (1993). Principles and Applications of Aquatic Chemistry. New York., Wiley Interscience.

Morel, F. M. M., A. M. L. Kraepiel and M. Amyot (1998). "The chemical cycle and bioaccumulation of mercury." Annual Review of Ecology and Systematics **29**: 543-566.

Morse, J. W. (1994). "Interactions of Trace-Metals with Authigenic Sulfide Minerals - Implications for Their Bioavailability." Marine Chemistry **46**(1-2): 1-6.

Morse, J. W. and T. Arakaki (1993). "Adsorption and Coprecipitation of Divalent Metals with Mackinawite (Fes)." Geochimica Et Cosmochimica Acta **57**(15): 3635-3640.

Morse, J. W. and G. W. Luther (1999). "Chemical influences on trace metal-sulfide interactions in anoxic sediments." Geochimica Et Cosmochimica Acta **63**(19-20): 3373-3378.

Navarro, A., H. Biester, J. L. Mendoza and E. Cardellach (2006). "Mercury speciation and mobilization in contaminated soils of the Valle del Azogue Hg mine (SE, Spain)." Environmental Geology **49**(8): 1089-1101.

Paquette, K. E. and G. R. Helz (1997). "Inorganic speciation of mercury in sulfidic waters: The importance of zero-valent sulfur." Environmental Science & Technology **31**(7): 2148-2153.

Piao, H. S. and P. L. Bishop (2006). "Stabilization of mercury-containing wastes using sulfide." Environmental Pollution **139**(3): 498-506.

Pierce, C. (2007). "Mercury in the Environment and Water Supply." from http://www.uwec.edu/piercech/Hg/mercury_water/cycling.htm.

Rickard, D. T. (1969). "The Chemistry of Iron Sulphide Formation at Low Temperatures." Stockholm Contributions to Geology **26**: 67-95.

Salatas, J. H., Y. W. Lowney, R. A. Pastorok, R. R. Nelson and M. V. Ruby (2004). "Metals that drive health-based remedial decisions for soils at US Department of Defense sites." Human and Ecological Risk Assessment **10**(6): 983-997.

Solomon, D. K., G. K. Moore, L. E. Toral, R. B. Dreier and W. M. McMaster (1992). A Hydraulic Framework for the Oak Ridge Reservation. Oak Ridge, TN, Oak Ridge National Laboratory.

Sparks, D. L. (1989). Kinetics of soil chemical processes. San Diego, Academic Press.

Stein, E. D., Y. Cohen and A. M. Winer (1996). "Environmental distribution and transformation of mercury compounds." Critical Reviews in Environmental Science and Technology **26**(1): 1-43.

Svensson, M., B. Allard and A. Duker (2006a). "Formation of HgS- mixing HgO or elemental Hg with S, FeS or FeS2." Science of the Total Environment **368**(1): 418-423.

Svensson, M., A. Duker and B. Allard (2006b). "Formation of cinnabar - estimation of favourable conditions in a proposed Swedish repository." Journal of Hazardous Materials **136**(3): 830-836.

Tiffreau, C., J. Lutzenkirchen and P. Behra (1995). "Modeling the Adsorption of Mercury(Ii) on (Hydr)Oxides .1. Amorphous Iron-Oxide and Alpha-Quartz." Journal of Colloid and Interface Science **172**(1): 82-93.

Toride, N., F. J. Leij and M. T. van Genuchten (1999). The CXTFIT Code for Estimating Transport Parameters from Laboratory or Field Tracer Experiments. Riverside, U.S. Department of Agriculture**:** 121.

USEPA (1997). EPA mercury study report to Congress. O. o. A. Q. a. S. a. O. o. R. a. Development. Washington, D.C., U.S. Environmental Protection Agency.

USEPA. (2006). "List of Drinking Contaminants & their MCLs ", from http://www.epa.gov/safewater/contaminants/dw_contamfs/mercury.html.

Viessman, W. and M. Hammer (1998). Water Supply and Pollution Control, Prentice Hall.

Walcarius, A., J. Devoy and J. Bessiere (1999). "Electrochemical recognition of selective mercury adsorption on minerals." Environmental Science & Technology **33**(23): 4278-4284.

Weber, W. J. (2001). Environmental systems and processes: principles, modeling, and design. New York:, Wiley-Interscience.

Willet, K. L., R. R. Turner, and J. J. Beauchamp (1992). "Effect of chemical form of mercury on the performance of dosed soils in standard leaching protocols: EP and TCLP." Hazardous Waste and Hazardous Materials **9**: 275-288.

Wolfenden, S., J. M. Charnock, J. Hilton, F. R. Livens and D. J. Vaughan (2005). "Sulfide species as a sink for mercury in lake sediments." Environmental Science & Technology **39**(17): 6644-6648.

Yudovich, Y. E. and M. P. Ketris (2005). "Mercury in coal: a review Part 2. Coal use and environmental problems." International Journal of Coal Geology **62**(3): 135-165.

APPENDICES

Appendix A. Sample Calculations

Example 1

Example calculation to determine removal efficiency and K_d in batch experiments.

Given: 2 g L^{-1} of pyrite, 2.5 mL 100 μM $Hg(II)_0$; 0.5 mL 0.05 M NaOH, 20mL H_20.

$$\text{Theoretical Hg(II)}_0 = \frac{2.5mL * 100\frac{\mu mol}{L} * 200\frac{\mu g}{\mu mol}}{2.5mL + 0.5mL + 20mL} = 2175\frac{\mu g}{L}$$

$$\text{Actual Hg(II)}_0 = \sum\frac{[Spikes]}{3} = \frac{2204\frac{\mu g}{L} + 2197\frac{\mu g}{L} + 2186\frac{\mu g}{L}}{3} = 2195\frac{\mu g}{L}$$

Removal Efficiency =

$$\frac{[Hg(II)_0] - [Hg(II)_i]}{[Hg(II)_0]} * 100\% = \frac{2195\frac{\mu g}{L} - 365\frac{\mu g}{L}}{2195\frac{\mu g}{L}} * 100\% = 83.4\%$$

Solid phase Hg(II) concentration (q) =

$$\frac{[Hg(II)_0] - [Hg(II)_i]}{Pyrite} = \frac{2195\frac{\mu g}{L} - 365\frac{\mu g}{L}}{2\frac{g}{L}} = 915\frac{\mu g.Hg(II)}{g.pyrite}$$

$$\text{Distribution coefficient } (K_d) = \frac{q}{Hg(II)_i} = \frac{915\frac{\mu g}{g}}{365\frac{\mu g}{L}} = 2.5\frac{L}{g} = 2510\frac{mL}{g}$$

Example 2

Example calculation to determine K_d and R in column experiments.

Given: 0.0625 g pyrite, 103.5 μg L^{-1} $Hg(II)_0$, 253 mL V_T,

From equation 3.4

$$q = \frac{\left(103.5\frac{\mu g}{L}(0.39L) - 24\mu g\right)}{0.0625g} = 260\frac{\mu g}{g}$$

From equation 3.7:

$$K_d = \frac{260\frac{\mu g}{g}}{103.5\frac{\mu g}{L}} = 2.5\frac{L}{g} = 2515\frac{mL}{g}$$

From equation 3.6:

$$K_p = 0.0095 * 2515\frac{mL}{g} = 0.024\frac{mL}{g}$$

From equation 3.5:

$$R = 1 + \frac{1.67\frac{g}{mL}}{0.37} * 0.024\frac{mL}{g} = 108$$

Appendix B. VisualMINTEQ Calculations.

B.1. Hg(II) Speciation.
Speciation of 2 mg L^{-1} Hg(II) at 0.1 M NaCl as a function of pH.

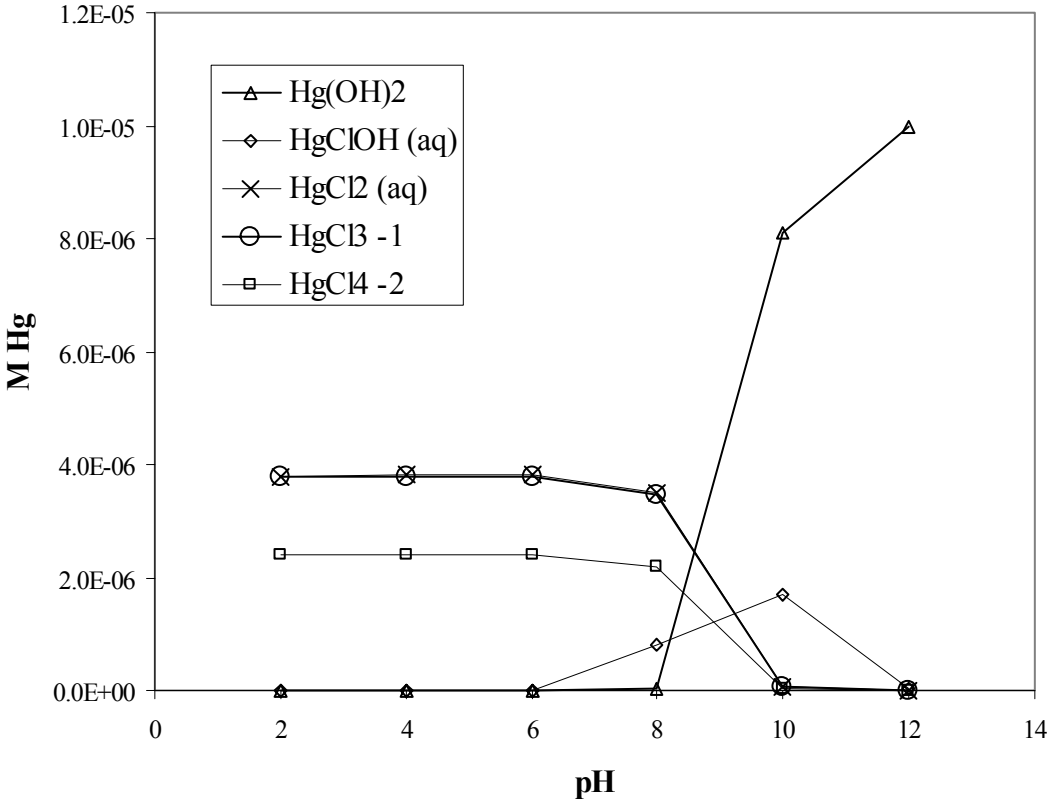

B.2. FeS(s) Solubility.
System consists of 2 mg L^{-1} Hg(II) and 2 g L^{-1} FeS(s) at 0.1 M NaCl as a function of pH.

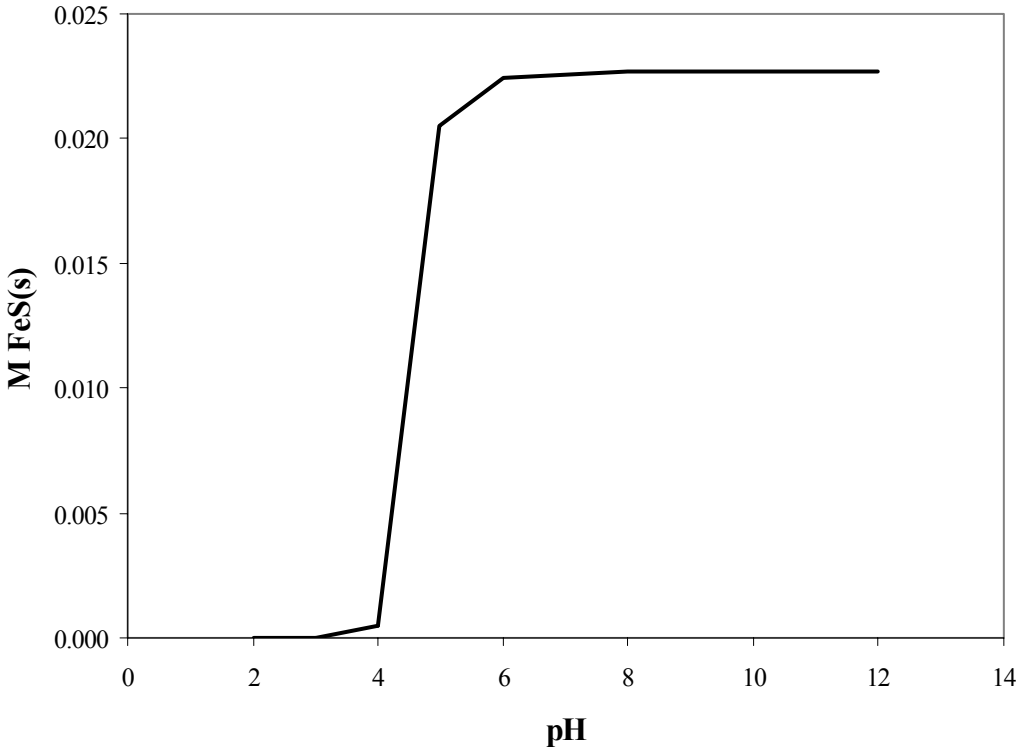

B.3. Hg(II) Speciation.

Speciation of 2 mg L^{-1} Hg(II) containing 2 g L^{-1} FeS(s) at 0.1 M NaCl as a function of pH.

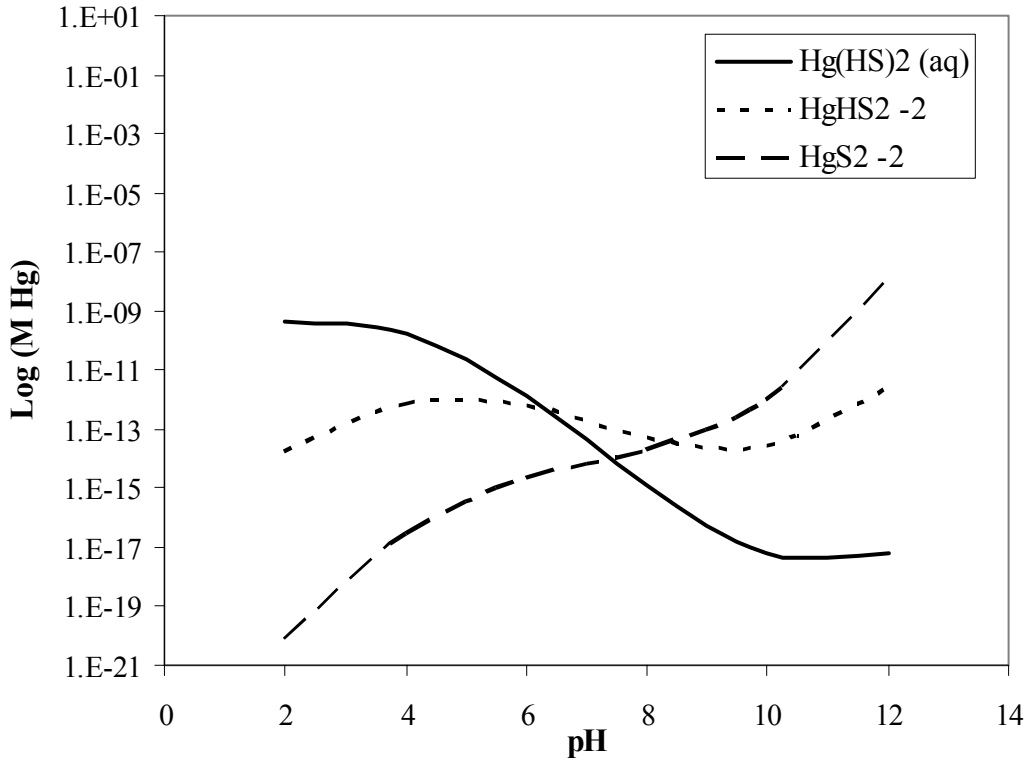

B.4. Solid Formation.
System consists of 2 mg L^{-1} Hg(II) and 2 g L^{-1} FeS(s) at 0.1 M NaCl as a function of pH.